Cell Metabolism
Clinical and Translational Report

The NADPARK study: A randomized phase I trial of nicotinamide riboside supplementation in Parkinson's disease

Graphical abstract

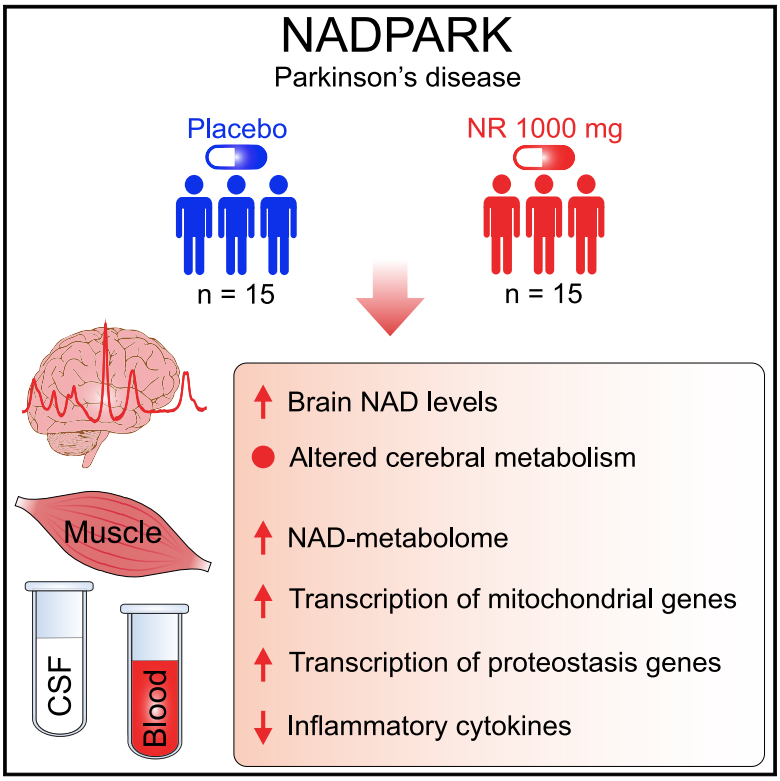

Highlights

- Oral NR increases brain NAD levels in individuals with Parkinson's disease
- NR intake alters cerebral metabolism in Parkinson's disease
- Cerebral NAD increase is associated with clinical improvement in Parkinson's disease
- NR induces transcription of mitochondrial, lysosomal, and proteasomal pathways

Authors

Brage Brakedal, Christian Dölle, Frank Riemer, ..., Renate Grüner, David Eidelberg, Charalampos Tzoulis

Correspondence

charalampos.tzoulis@uib.no

In brief

Researchers from Haukeland University Hospital conducted a phase I trial of NAD-replenishment therapy with oral nicotinamide riboside (NR) in Parkinson's disease (PD). NR increased cerebral NAD levels, and this was associated with altered brain metabolism and clinical improvement. The findings nominate NR as a potential neuroprotective treatment for PD.

Brakedal et al., 2022, Cell Metabolism *34*, 396–407
March 1, 2022
https://doi.org/10.1016/j.cmet.2022.02.001

CellPress

CellPress
OPEN ACCESS

Cell Metabolism

Clinical and Translational Report

The NADPARK study: A randomized phase I trial of nicotinamide riboside supplementation in Parkinson's disease

Brage Brakedal,[1,2,9] Christian Dölle,[1,2,9] Frank Riemer,[1,3,10] Yilong Ma,[4,10] Gonzalo S. Nido,[1,2] Geir Olve Skeie,[1,2] Alexander R. Craven,[3,5,6] Thomas Schwarzlmüller,[2,7] Njål Brekke,[3] Joseph Diab,[8] Lars Sverkeli,[8] Vivian Skjeie,[7] Kristin Varhaug,[1,2] Ole-Bjørn Tysnes,[1,2] Shichun Peng,[4] Kristoffer Haugarvoll,[1,2] Mathias Ziegler,[1,8] Renate Grüner,[3] David Eidelberg,[4] and Charalampos Tzoulis[1,2,11,*]

[1]Neuro-SysMed, Department of Neurology, Haukeland University Hospital, Bergen, Norway
[2]Department of Clinical Medicine, University of Bergen, Bergen, Norway
[3]Mohn Medical Imaging and Visualization Centre (MMIV), Department of Radiology, Haukeland University Hospital, Bergen, Norway
[4]Center for Neurosciences, Institute of Molecular Medicine, The Feinstein Institutes for Medical Research, Manhasset, NY, USA
[5]Department of Biological and Medical Psychology, University of Bergen, Bergen, Norway
[6]Department of Clinical Engineering, Haukeland University Hospital, Bergen, Norway
[7]Department of Radiology, Haukeland University Hospital, Bergen, Norway
[8]Department of Biomedicine, University of Bergen, Bergen, Norway
[9]These authors contributed equally
[10]These authors contributed equally
[11]Lead contact
*Correspondence: charalampos.tzoulis@uib.no
https://doi.org/10.1016/j.cmet.2022.02.001

SUMMARY

We conducted a double-blinded phase I clinical trial to establish whether nicotinamide adenine dinucleotide (NAD) replenishment therapy, via oral intake of nicotinamide riboside (NR), is safe, augments cerebral NAD levels, and impacts cerebral metabolism in Parkinson's disease (PD). Thirty newly diagnosed, treatment-naive patients received 1,000 mg NR or placebo for 30 days. NR treatment was well tolerated and led to a significant, but variable, increase in cerebral NAD levels—measured by ^{31}phosphorous magnetic resonance spectroscopy—and related metabolites in the cerebrospinal fluid. NR recipients showing increased brain NAD levels exhibited altered cerebral metabolism, measured by ^{18}fluoro-deoxyglucose positron emission tomography, and this was associated with mild clinical improvement. NR augmented the NAD metabolome and induced transcriptional upregulation of processes related to mitochondrial, lysosomal, and proteasomal function in blood cells and/or skeletal muscle. Furthermore, NR decreased the levels of inflammatory cytokines in serum and cerebrospinal fluid. Our findings nominate NR as a potential neuroprotective therapy for PD, warranting further investigation in larger trials.

INTRODUCTION

Parkinson's disease (PD) affects 1%–2% of the population above the age of 65 and is a major cause of death and disability, with a rapidly growing global socioeconomic impact (Gooch et al., 2017; de Rijk et al., 2000). Current treatments for PD can provide partial symptomatic relief, mainly for motor symptoms but make no substantial impact on disease progression (Athauda and Foltynie, 2015; Bloem et al., 2021; Kalia and Lang, 2015). Despite several candidate neuroprotective therapies showing encouraging preclinical results, these have failed to show disease-modifying effects in clinical trials (Athauda and Foltynie, 2015; Espay et al., 2017).

A growing body of evidence supports that boosting cellular levels of nicotinamide adenine dinucleotide (NAD) may confer neuroprotective effects in both healthy aging and neurodegeneration (Lautrup et al., 2019). NAD is reversibly interconverted between its oxidized (NAD^+) and reduced (NADH) state and thereby constitutes an essential cofactor for metabolic redox reactions, including mitochondrial respiration. Furthermore, NAD^+ is substrate to vital signaling reactions involved in DNA repair, histone and other protein deacylation reactions, and second messenger generation (Katsyuba et al., 2020). These reactions consume NAD^+ at high rates, requiring constant replenishment via NAD biosynthesis. NAD levels have been shown to decline with age and this is believed to contribute to age-related diseases (Johnson and Imai, 2018; Katsyuba et al., 2020). Increasing the NAD-replenishment rate (e.g., via supplementation of precursors) and/or enhancing the NAD^+/NADH ratio (e.g., via caloric restriction) have shown beneficial effects on lifespan and healthspan in

CellPress
OPEN ACCESS

Table 1. Demographic and anamnestic information

	Placebo (n = 15)	NR (n = 15)	MRS responders[a] (n = 10)
Sex (male/female)	14/1	11/4	8/2
Mean age	63.7 ± 11.0	63.9 ± 8.0	63.2 ± 9.8
Height (cm)	179.0 ± 6.0	176.9 ± 7.8	179.3 ± 7.6
Weight (kg)	83.6 ± 11.7	83.0 ± 14.0	87.1 ± 10.1
Drug compliance, %	98.53 ± 0.99	97.3 ± 2.38	96.9 ± 2.7
Time on study drug (days)	32.4 ± 2.5	32.5 ± 2.7	32.5 ± 2.5
MDS diagnosis[b] (established/probable)	5/10	9/6	6/4
Anamnestic loss of smell (yes/no)	9/6	12/3	7/3
Anamnestic RBD[c] (yes/no)	4/11	3/12	3/7
Anamnestic PD symptoms[d] (months)	20.3 ± 13.2	26.6 ± 11.5	27.8 ± 12.3

[a]Magnetic resonance spectroscopy responders
[b]Movement Disorder Society clinical diagnostic criteria
[c]Rapid eye movement sleep behavior disorder
[d]Time from first subjective symptom of parkinsonism to visit 1

multiple model systems and provided evidence of neuroprotection in animal models of neurodegeneration and other age-related diseases (Braidy and Liu, 2020; Johnson and Imai, 2018; Katsyuba et al., 2020)

Enhancing NAD replenishment could potentially help ameliorate several major processes implicated in the pathogenesis of PD, including mitochondrial respiratory dysfunction (Fløngs et al., 2018; Hattori et al., 1991; Schapira et al., 1989), neuroinflammation (Hirsch and Hunot, 2009), epigenomic dysregulation (Park et al., 2016; Toker et al., 2021), and increased neuronal DNA damage (Gonzalez-Hunt and Sanders, 2021).

NAD can be replenished via supplementation of nicotinamide riboside (NR), a vitamin B3 molecule and biosynthetic precursor of NAD (Bieganowski and Brenner, 2004; Katsyuba et al., 2020). NR has undergone extensive preclinical testing (Conze et al., 2016) and is well tolerated by adult humans, showing no evidence of toxicity with doses up to at least 2,000 mg daily (Dollerup et al., 2018). Trials in healthy individuals have shown that an oral intake of 1,000 mg NR daily substantially elevates total levels of NAD and related metabolites in blood and muscle, boosts mitochondrial bioenergetics, and decreases circulating inflammatory cytokines (Conze et al., 2019; Elhassan et al., 2019; Martens et al., 2018; Trammell et al., 2016). Moreover, evidence from cell and animal studies suggests that NR supplementation promotes health span and has neuroprotective effects in models of Cockayne syndrome (Okur et al., 2020), noise-induced injury (Brown et al., 2014; Han et al., 2020), amyotrophic lateral sclerosis (Harlan et al., 2020), Alzheimer's disease (Sorrentino et al., 2017; Xie et al., 2019), and PD (Schöndorf et al., 2018).

Taken together, this evidence suggests that NR may hold promise as a potential neuroprotective agent for PD. However, several critical knowledge gaps have yet to be addressed. Specifically, it needs to be established whether NR is well tolerated, augments cerebral NAD levels, and affects cerebral metabolism in patients with PD.

To address these questions, we conducted a double-blinded, randomized, placebo-controlled phase I study of NR in newly diagnosed PD patients, naive to dopaminergic therapy (the NADPARK study, Clinicaltrials.gov: NCT03816020). Primary outcomes were the detection of cerebral penetration and metabolic response, measured by ^{31}phospohorous-magnetic resonance spectroscopy (^{31}P-MRS), cerebrospinal fluid (CSF) metabolomics, and ^{18}fluoro-deoxyglucose positron emission tomography (FDG-PET). Secondary outcomes were the safety and tolerability of NR in the study population (measured by the frequency and severity of adverse events and changes in vital signs and clinical laboratory values), the impact of NR on clinical symptoms (measured using the Movement Disorder Society unified Parkinson's disease rating scale [MDS-UPDRS]), and the impact of NR on the NAD metabolome in peripheral tissues of PD patients. We found that NR supplementation was well tolerated with no adverse effects. Treatment increased brain NAD levels, as well as related metabolites in the CSF and peripheral tissues. At the individual level, the increase in cerebral NAD was not universal but evident in 10/13 NR recipients from whom data were available. The NR recipients who showed increased brain NAD levels exhibited altered cerebral metabolism, inducing a specific treatment-related metabolic network that overlapped with key elements of the PD-related spatial covariance pattern (PDRP) (Schindlbeck and Eidelberg, 2018) and were associated with mild clinical improvement.

Our findings suggest that NR may be useful as a neuroprotective therapy in PD, pending further investigation in a phase II study.

RESULTS

In total, 36 patients were screened, and 30 eligible patients were enrolled, all of whom completed the study (Figure S1). There were no significant demographic differences between the NR and placebo group (Table 1). Seven subjects in the NR group and three subjects in the placebo group reported adverse events, all of which were minor and considered to be unrelated to NR (Table S1). Based on the number of remaining capsules in returned vials, we estimated a mean study drug adherence in the NR and placebo group to be 98%. The average time on study drug was 32.5 (±2.7) days for the NR group and 32.4 (±2.53) days for the placebo group (Table S2). Four participants (two in the NR and two in the placebo group) did not return any capsules but reported they were drug compliant.

Table 2. MDS-UPDRS mean clinical scores

	Placebo (n = 15)	NR (n = 15)	MRS responders[a] (n = 10)
Mean score ± SD			
MDS-UPDRS[b] I			
Visit 1	6.3 ± 4.5	6.3 ± 4.0	6.2 ± 4.6
Visit 2	6.0 ± 3.7	5.4 ± 3.9	5.3 ± 4.3
MDS-UPDRS II			
Visit 1	7.5 ± 4.4	7.9 ± 4.3	6.4 ± 4.3
Visit 2	7.6 ± 4.6	8.3 ± 4.3	6.4 ± 3.8
MDS-UPDRS III			
Visit 1	27.0 ± 8.7	31.1 ± 10.0	29.6 ± 11.0
Visit 2	26.3 ± 11.0	30.5 ± 9.8	28.7 ± 10.6
Total score MDS-UPDRS (I–III)			
Visit 1	40.7 ± 13.3	45.2 ± 13.2	42.2 ± 15.3
Visit 2	39.9 ± 14.3	44.1 ± 13.2	40.4 ± 14.2
Hoehn and Yahr[c] stage			
Visit 1	1.9 ± 0.6	1.8 ± 0.4	1.7 ± 0.5
Visit 2	1.8 ± 0.6	1.9 ± 0.5	1.8 ± 0.4

[a]Magnetic resonance spectroscopy responders
[b]Movement Disorder Society unified Parkinson's disease rating scale
[c]Hoehn and Yahr rating scale

NR increases cerebral NAD levels

^{31}P-MRS was employed to assess phosphorylated metabolites in the patients' brain. At the end of the study, data were available from 27 individuals, including 13 in the NR group and 14 in the placebo group (Table S2). ^{31}P-MRS data analyses allowed for identification and quantitation of multiple phosphorylated compounds (Figures 1A–1C; Table S3). NAD levels, which were normalized to ATP-α, showed a significant increase in the NR group (paired t test, p = 0.016), but not in the placebo group (Figure 1D). Direct comparison between the groups showed that the between visit change (visit 2/visit 1) in the NAD/ATP-α ratio was significantly higher in the NR group compared with the placebo group (t test, p = 0.025). No other detected cerebral metabolites exhibited significant change in either the NR or placebo group between visits. At the individual level, the cerebral NAD response was heterogeneous, with 10/13 patients showing an increase, of whom 9 showed a change exceeding 10% of baseline levels. We will henceforth refer to the subgroup of 10 NR recipients who showed an increase in cerebral NAD levels as MRS responders. Since this variability raised the possibility of heterogeneous treatment effects, we chose to stratify downstream neurometabolic and clinical analyses.

NR induces a novel treatment-related metabolic network

We next interrogated the FDG-PET data of the NR recipients to determine whether treatment-related increases in cerebral NAD levels were associated with a significant metabolic brain network. To this end, we applied a supervised principal component analysis (PCA) algorithm (ordinal trends/canonical variates analysis [OrT/CVA]) to paired scan data from the NR participants (n = 10) for whom brain NAD levels were simultaneously increased with treatment. The analysis revealed a significant ordinal trend pattern, which was represented by the first principal component (PC1), accounting for 20.6% of the variance in the paired data. This NR-related metabolic pattern (NRRP; Figures 2A and S2) was characterized by bilateral metabolic reductions in the caudate and putamen, extending into the adjacent globus pallidus, and in the thalamus (Table S4). As part of the network, these changes were also associated with localized cortical reductions along the medial wall of the hemisphere involving the precuneus (Brodmann area [BA] 7), medial frontal cortex (BA 9 and 10), anterior cingulate area (BA 24 and 32), and in the posterior cingulate gyrus (BA 31). The reliability of these regions was demonstrated by bootstrap iteration (inverse coefficient of variation [ICV] z = −3.83, −2.58, p < 0.005; 1,000 iterations). Areas with relative metabolic increases did not contribute significantly to this topography.

At the individual subject level, a significant ordinal trend in NRRP expression was observed (p < 0.018; permutation test, 1,000 iterations) in the 10 NR recipients in the pattern identification group (Figure 2B, black lines; Figure 2C). Although analogous NR-mediated increases in pattern expression were not seen in the remaining 4 NR recipients who either did not exhibit NAD responses on MRS or for whom MRS data were not available (Figure 2B, gray lines), the ordinal trend remained significant for the NR group as a whole (p = 0.027). That said, consistent changes in NRRP expression were not significant in the placebo group (p = 0.497). Significant correlations were not observed between treatment-related changes in cerebral NAD levels and NRRP expression in either of the trial groups (p > 0.10).

Nevertheless, changes in NRRP expression in the NR group correlated significantly (r = −0.59, p = 0.026) with the changes in UPDRS motor ratings recorded at the time of PET (Figure 2D; Table S2). Thus, the largest NRRP increases were observed in the NR subjects with the greatest improvement in motor ratings. An analogous correlation was not seen in the placebo group (p = 0.79). We noted that certain NRRP regions were shared with the previously validated PDRP topography (Figure 2E, top; Figure S2, middle). In particular, areas of reduced activity in the caudate and putamen, extending into the adjacent globus pallidus, overlapped with corresponding areas of overactivity in the PDRP (Figure 2E, bottom, hot voxels; Figure S2). Likewise, spatial overlap was observed between underactive regions in the frontal and parietal cortex for the two patterns (Figure 2E, bottom, purple voxels; Figure S2, bottom). Indeed, a significant correlation was observed between baseline PDRP and NRRP expression values across the trial population (r = 0.56, p = 0.002; Figure 2F). As typically seen in PD populations, PDRP expression values at baseline correlated with UPDRS motor ratings (r = 0.374, p = 0.046 for the two groups; Figure 2G). In contrast to NRRP in which the changes in pattern expression with NR correlated with clinical improvement (Figure 2D), no correlation with outcome was observed for the PDRP changes (p = 0.73).

NR-induced increase in cerebral NAD is associated with clinical improvement of PD

No significant change was found in the MDS-UPDRS (total or subsections I–III) in the NR or placebo groups. However, a trend for decreased MDS-UPDRS was seen in the MRS-responder

CellPress
OPEN ACCESS

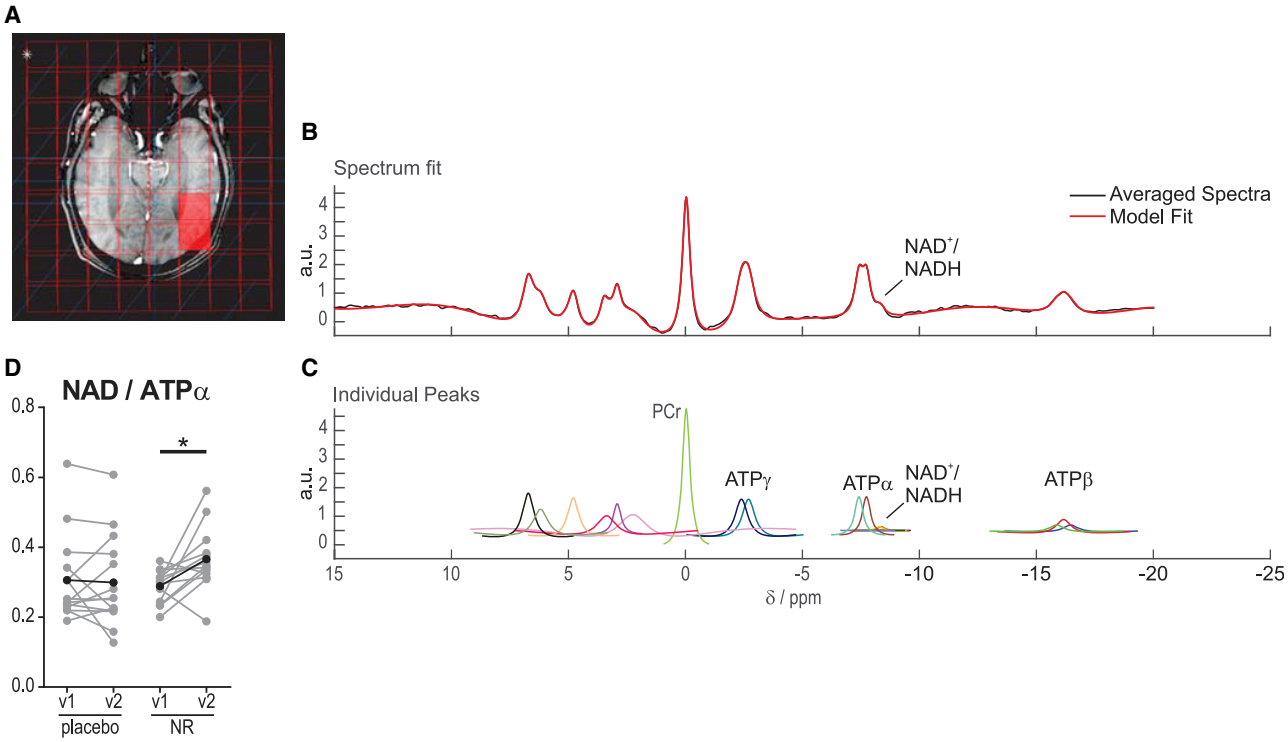

Figure 1. ^{31}P-MRS analysis reveals NR-mediated increase in cerebral NAD

(A–C) Exemplary data from one subject.

(A) Spectroscopy voxel position in the occipital cortex. Spectra were acquired for each grid position.

(B) Averaged processed spectra from several occipital lobe voxels in black. The model fit of the data is shown in red. The model fit is composed of the convolution of all spectral contributions of a simulated dataset fitted to the experimental data shown in (C). The position of NAD^+/NADH is indicated.

(C) Phosphocreatine (PCr) was chosen as the chemical shift reference at 0 ppm. Other detected phosphometabolites are indicated.

(D) Relative total NAD levels normalized to ATP-α at visit 1 and 2. Data points show individual measurements (gray) and averages (black).

*p = 0.0105 (Wilcoxon test).

subgroup (mean decrease 1.9 ± 2.78; paired t test, p = 0.071), and this reached statistical significance when only the 9 individuals showing >10% increase in cerebral NAD levels were considered (mean decrease 2.33 ± 2.35; paired t test, p = 0.017). Upon closer inspection, this effect appeared to be mainly driven by subsections I and III of the MDS-UPDRS. The clinical scores of the participants at each visit are shown in Tables 2 and S2.

NR supplementation augments the NAD metabolome in the CSF and peripheral tissues of PD patients

Metabolomic analyses were carried out in CSF, skeletal muscle, and peripheral blood mononuclear cells (PBMCs) to confirm NR intake and investigate potential changes in related metabolic pathways. In CSF, we detected a substantial increase of the nicotinamide (Nam) degradation product N-methyl-2-pyridone-5-carboxamide (Me-2-PY), an established indicator of NR supplementation (Elhassan et al., 2019; Trammell et al., 2016) (Figure 3) in all NR recipients. Other related metabolites, including NAD^+, NADH, nicotinamide mononucleotide (NMN), nicotinic acid adenine dinucleotide (NAAD), and methyl nicotinamide (Me-Nam), were below the detection limit in the CSF. This finding further corroborated that oral NR therapy increases brain NAD levels across the blood brain barrier, as indicated by the ^{31}P-MRS data. In muscle tissue, several NAD-related metabolites, including Nam degradation products nicotinamide N-oxide (Nam N-oxide), Me-Nam, and the methyl pyridones (Me-2-PY) and N-methyl-4-pyridone-5-carboxamide (Me-4-PY), as well as the acid form of NAD, NAAD, were strongly elevated after treatment with NR (Figure 3). The steady-state levels of NAD itself (both oxidized NAD^+ and reduced NADH), and NAD precursors and intermediates, were not significantly changed by NR treatment (Figure S3), similar to reports from previous trials in humans (Elhassan et al., 2019). PBMCs showed less extensive changes, recapitulating the increase in NAAD and Me-Nam (Figures 3 and S4). Additional metabolites that could potentially be affected by changes in the NAD metabolome were investigated, including acetyl-CoA and CoA, the methyl donor S-adenosylmethionine (SAM) and its metabolites, and energy compounds, such as ATP. These showed no significant change in PBMCs or muscle (Figures S3 and S4). Importantly, substantial metabolic changes were seen in the entire NR group in all tissues, irrespective of the cerebral NAD response in ^{31}P-MRS.

NR therapy induces the expression of mitochondrial, antioxidant, and proteostatic processes

To investigate the effects of NR therapy on gene expression, we carried out RNA-seq analysis in PBMCs and muscle tissue from all study participants and assessed the between visit differences

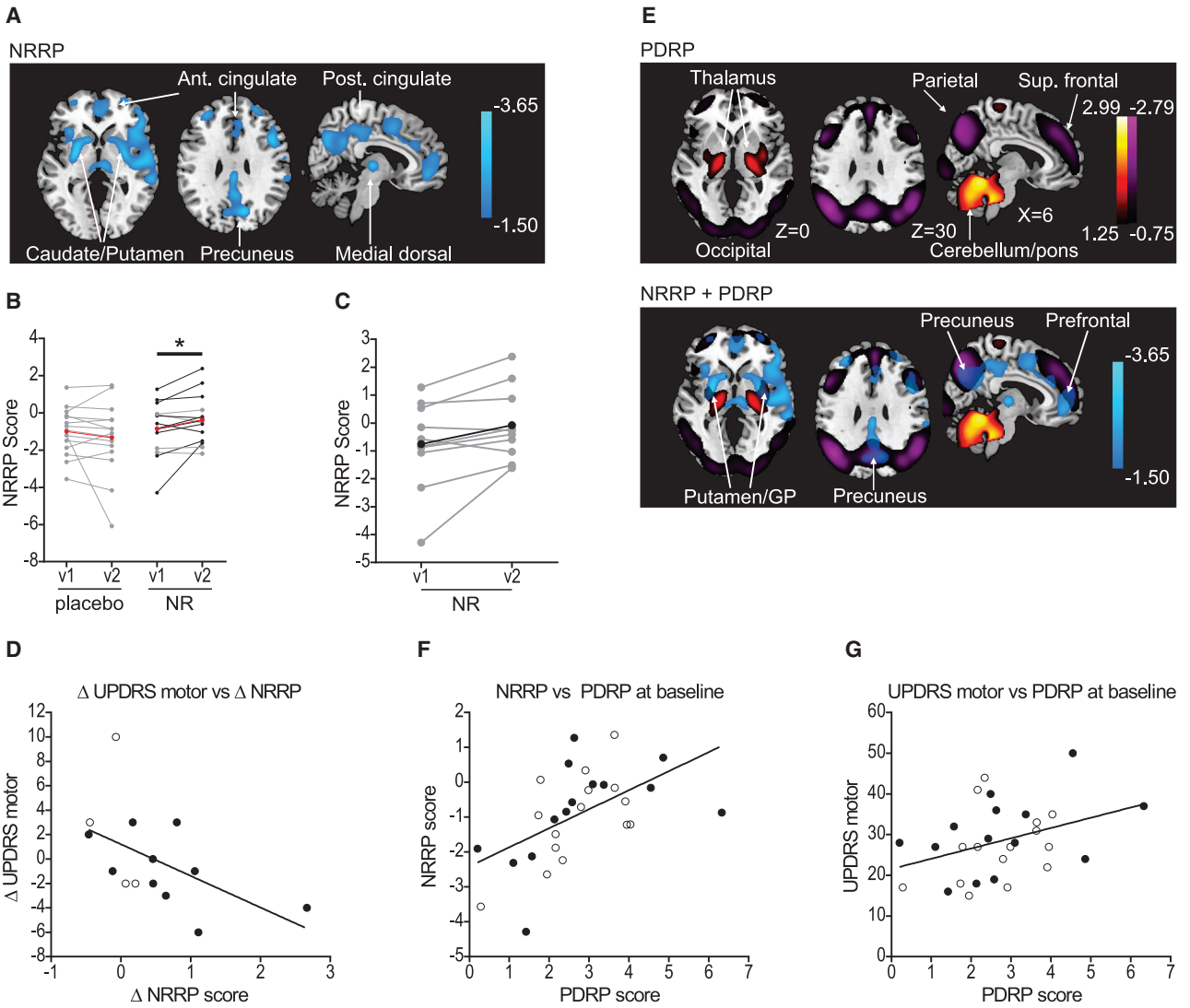

Figure 2. Metabolic brain network topography associated with NR treatment

(A) NR-related metabolic pattern (NRRP) identified with FDG-PET in MRS responders with negative loading (blue). The values of region weight were thresholded at a Z value of −1.5.

(B) Between visit changes showing increased NRRP expression in the NR versus the placebo group. The red line indicates mean values before and after the treatment. Black lines indicate individuals with a positive NAD response in the MRS analysis. Gray lines indicate the remaining individuals (i.e., the 4 individuals who either showed no NAD response in the MRS [n = 2] or for whom MRS data were not available [n = 2]; see also Table S3). *p = 0.027 (permutation test, 1,000 iterations).

(C) Changes in NRRP expression in the MRS responders treated with NR. NRRP expression increased in 8 of 10 subjects (p = 0.018, permutation test, 1,000 iterations) showing elevated occipital NAD levels. Individual (gray lines) and average values (black line) are shown.

(D) NR-related changes in UPDRS motor ratings and NRRP expression correlated in the NR group (r = −0.590, p = 0.026), including the MRS responders (filled circles) and the others (open circles). The correlation was still significant (r = −0.556, p = 0.048) after excluding the data point with the greatest increase in UPDRS motor score at the top left corner of the graph.

(E) Top: PD-related metabolic pattern (PDRP) with positive (hot) and negative (purple) loadings previously identified with FDG-PET in the American patient population (Peng et al., 2014; Schindlbeck and Eidelberg, 2018). Bottom: composite imaging display showing overlap in putamen and pallidum or prefrontal cortex and precuneus between NRRP (blue) and PDRP (hot or purple).

(F and G) Correlations of NRRP and PDRP expression scores at baseline (r = 0.546, p = 0.002) and corresponding UPDRS motor ratings and PDRP expression at baseline (r = 0.374, p = 0.046) in the combined NR (filled circles) and PL (open circles) group.

in the NR group compared with the placebo group. In muscle tissue, NR supplementation was significantly associated with differential expression of 58 genes (FDR < 0.05; Table S5). These included substantial upregulation of *KLF2*, which is associated with decreased adipogenesis and induction of the nuclear factor erythroid 2-related factor 2 (Nrf2), a transcription factor with a key role in protection against oxidative damage, which has been linked to PD (Petrillo et al., 2020). We also noted

CellPress
OPEN ACCESS

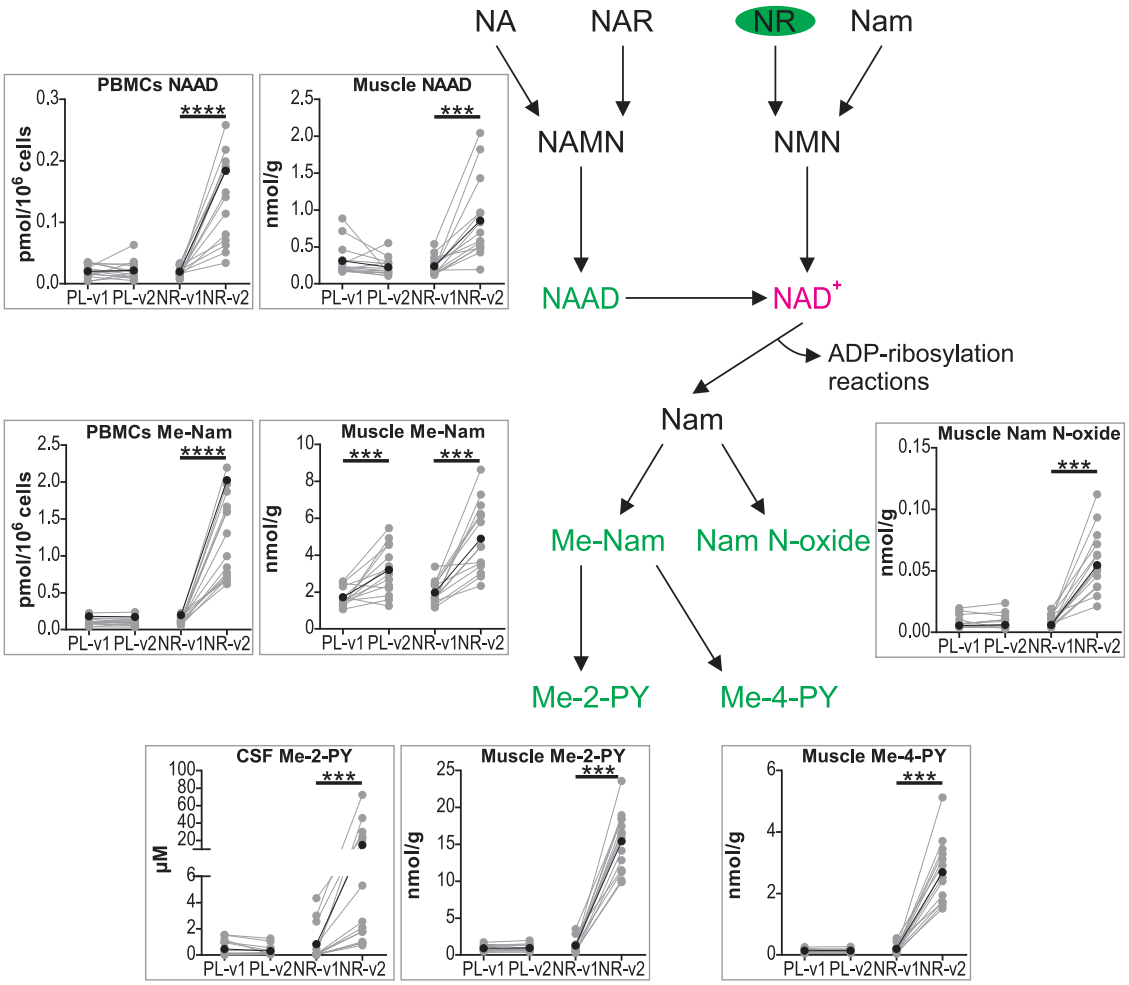

Figure 3. NR augments the NAD metabolome in CSF and peripheral tissues of PD patients

The graph shows NAD^+ biosynthesis and degradation routes, including precursors, intermediates, and catabolic end products. Boxed plots show concentrations in placebo and NR-treated individuals at visit 1 and visit 2 for those detectable metabolites that changed significantly with treatment in muscle, PBMCs, and CSF. Metabolites that changed significantly with NR treatment are highlighted in green. Data points show individual measurements (gray) and averages (black).

NA, nicotinic acid; NAR, nicotinic acid riboside; Nam, nicotinamide; NR, nicotinamide riboside; NAMN, nicotinic acid mononucleotide; NMN, nicotinamide mononucleotide; NAAD, nicotinic acid adenine dinucleotide; NAD^+, nicotinamide adenine dinucleotide; Me-Nam, methyl nicotinamide; Nam N-oxide, nicotinamide N-oxide; Me-2-PY, N-methyl-2-pyridone-5-carboxamide; Me-4-PY, N-methyl-4-pyridone-5-carboxamide.

*$p < 0.05$, **$p < 0.01$, ***$p < 0.001$, ****$p < 0.0001$ (Wilcoxon test).

upregulation of genes linked to NAD-degradation, such as ADP-ribosylation (*PARP15*), and NAD-dependent redox processes, such as the glycine cleavage system (*AMT*), as well as mitochondrial translation and respiratory complex assembly (*FARS2*, *TMEM242*). Gene set enrichment analyses revealed NR-induced upregulation of biological processes, including proteasomal function, and RNA transport and stability. In PBMCs, a total of 13 genes were significantly associated with NR supplementation, including upregulation of *BLOC1S2*, a component of the BLOC-1 complex involved in lysosomal biogenesis and trafficking (Starcevic and Dell'Angelica, 2004). Functional enrichment revealed highly significant upregulation of multiple biological processes, including ribosomal, proteasomal, lysosomal, and mitochondrial (oxidative phosphorylation) pathways. A complete account of NR-regulated pathways is provided in Table S6. No significant changes were found in genes encoding known NAD biosynthetic enzymes, including *NMRK1*, encoding nicotinamide riboside kinase 1, which converts NR to NMN. Finally, NR treatment did not show a significant association with estimated cell type proportions in the PBMC samples ($p > 0.5$, visit:treatment interaction term, linear mixed model, Welch-Satterthwaite's t test, $p < 0.05$; Figure S5).

NR modulates biomarkers of inflammation and mitochondrial dysfunction

Since mitochondrial dysfunction (Flønes et al., 2018; Hattori et al., 1991; Schapira et al., 1989) and inflammation (Hirsch and Hunot, 2009) have been associated with the pathophysiology of PD, we sought to identify NR-induced changes in relevant biomarkers in the serum and CSF of our patients. We assessed the levels of growth factors FGF21 and GDF15, which have been associated with mitochondrial dysfunction (Boenzi

and Diodato, 2018; Lehtonen et al., 2016), and a panel of 35 inflammatory cytokines. Growth factor analysis revealed a mild but significant decrease of GDF15 levels in the serum, but not in the CSF. FGF21 was unchanged in the serum and was below detection limit in CSF. Several inflammatory cytokines decreased in the serum and/or CSF of the NR-treated group (Figures 4 and S6). Notably, several of the serum cytokines also showed a significant decrease in the placebo group. Comparing the fold change of those cytokines between the groups revealed no significant difference (Figure S6A). In addition, we assessed the levels of neurofilament light chain (Nf-L), which are indicative of neuronal damage. These were unchanged by NR treatment in both the serum and CSF.

DISCUSSION

We present the results of the first NR trial in PD. Our study met its primary outcome, which was to assess penetration and metabolic responses of the brain in patients with PD. We established that orally administered NR is safe, leads to an increase in cerebral NAD levels, and alters cerebral metabolism in patients with PD. Cerebral penetration was further validated by detecting an increase of the metabolite Me-2-PY in the CSF of participants receiving NR, but not in the placebo. Furthermore, NR augmented the NAD metabolome and increased the expression of genes related to mitochondrial, lysosomal, and proteasomal function in blood and muscle and decreased the levels of inflammatory cytokines in serum and CSF.

Although a significant increase in cerebral NAD levels was detected by ^{31}P-MRS in the NR group, this effect was not universal. Three patients showed no evidence of cerebral NAD increase, despite a clear metabolic response in CSF, blood, and muscle, thereby confirming treatment compliance and an impact on the NAD metabolome. The fact that we detected an increase of Me-2-PY in the CSF of all NR recipients suggests that central nervous system penetration was universal. Thus, the variable cerebral NAD response observed by ^{31}P-MRS is likely to reflect interindividual variability in cerebral NAD metabolism and, possibly, limited sensitivity of the NAD measurement by MRS (i.e., MRS non-responders may have a positive, but mild cerebral NAD increase, which is below the detection limits of the method). Irrespective of the mechanisms underlying this variable response, our findings indicate that assessment of cerebral NAD levels may be an important monitoring parameter in clinical trials evaluating NR supplementation for brain health and disease. Variability in the achieved NAD increase in the patient brain raises the possibility of a heterogeneous biological and, potentially, clinical response to NR therapy. Increase in cerebral NAD levels was indeed associated with both neurometabolic and clinical response in our patients. Notably, a trend for clinical improvement, in the form of decreased MDS-UPDRS score, was seen in the subgroup of NR recipients who had an increase in cerebral NAD levels by ^{31}P-MRS.

FDG-PET analyses identified the NRRP—a novel network topography that was induced in PD trial participants receiving NR, but not placebo, under blinded conditions. Apart from its defining ordinal trend, changes in pattern expression with NR correlated with clinical improvement as measured by reductions in MDS-UPDRS ratings. The NRRP consisted mainly of decreased glucose uptake in the basal ganglia and neocortical areas. This may reflect a more efficient bioenergetic state, requiring less glucose consumption to maintain required ATP production. Increased NAD^+ levels would promote fatty acid beta-oxidation (Akie et al., 2015; Guarino and Dufour, 2019; Mukherjee et al., 2017), thereby providing an increased supply of reducing equivalents (i.e., NADH, $FADH_2$) to the respiratory chain independent of glycolysis. While the organization of the NRRP remains unknown at the systems level, the network shares a number of topographic features with the PDRP, which support a potential role for NR in PD therapeutics. The overlap between metabolically active PDRP regions in the posterior putamen and globus pallidus and areas of treatment-related metabolic reduction in the NRRP is particularly relevant. In recent graph theoretic studies of PDRP organization, we found that these regions comprise a discrete core zone, which drives overlap network activity. Metabolic reductions in core nodes have been observed in symptomatic PD treatments, such as levodopa administration and subthalamic deep brain stimulation (Asanuma et al., 2006; Niethammer and Eidelberg, 2012). The presence of similar changes with NR suggests that these regions may also be modulated by this treatment. In any event, clinical outcomes in the NR group relate more to the induction of NRRP than to the modulation of the PDRP activity—a situation similar to that encountered with subthalamic gene therapy (Niethammer et al., 2018).

Metabolomic analyses in PBMCs and muscle confirmed NR intake in the treatment group and excluded this in the placebo group. Notably, a highly significant increase in established markers of NR-mediated NAD biosynthesis, such as NAAD and Me-Nam, was seen in all patients in the NR group, corroborating previous studies in healthy subjects (Elhassan et al., 2019). Measured NAD^+ values were substantially lower than previously reported concentrations in these tissues (Elhassan et al., 2019; Lamb et al., 2020; Martens et al., 2018; Trammell et al., 2016); however, we did not detect an increase in NAD^+ levels (Figures S3 and S4). It is conceivable that a new steady state of increased NAD flux may be established over time in muscle and blood cells without detectable changes in the measured NAD concentrations at any given time point. This could be due to increased NAD consumption combined with increased NAD biosynthesis, facilitated via continuous NR supply. Evidence of increased flux in the NAD metabolome was indeed detected in both PBMCs and muscle of our patients, indicating higher NAD availability in the NR group. Notably, unchanged NAD levels in muscle were also seen in a recent study of NR in healthy adults (Elhassan et al., 2019), whereas another study detected elevated NAD^+ levels in PBMCs (Trammell et al., 2016).

In addition to the NAD metabolome, we investigated other metabolites, which are functionally linked to NAD metabolism and signaling, and may be affected by NR treatment. Synthesis of Me-Nam, which was greatly increased by NR supplementation, requires the methyl donor SAM. This, in turn, could limit SAM availability for other essential methylation reactions, such as DNA and histone methylation, and neurotransmitter synthesis, including dopamine (Jadavji et al., 2015). We found no significant changes in SAM or its related metabolites SAH and homocysteine, indicating that NR supplementation does not limit SAM availability for other vital reactions.

CellPress
OPEN ACCESS

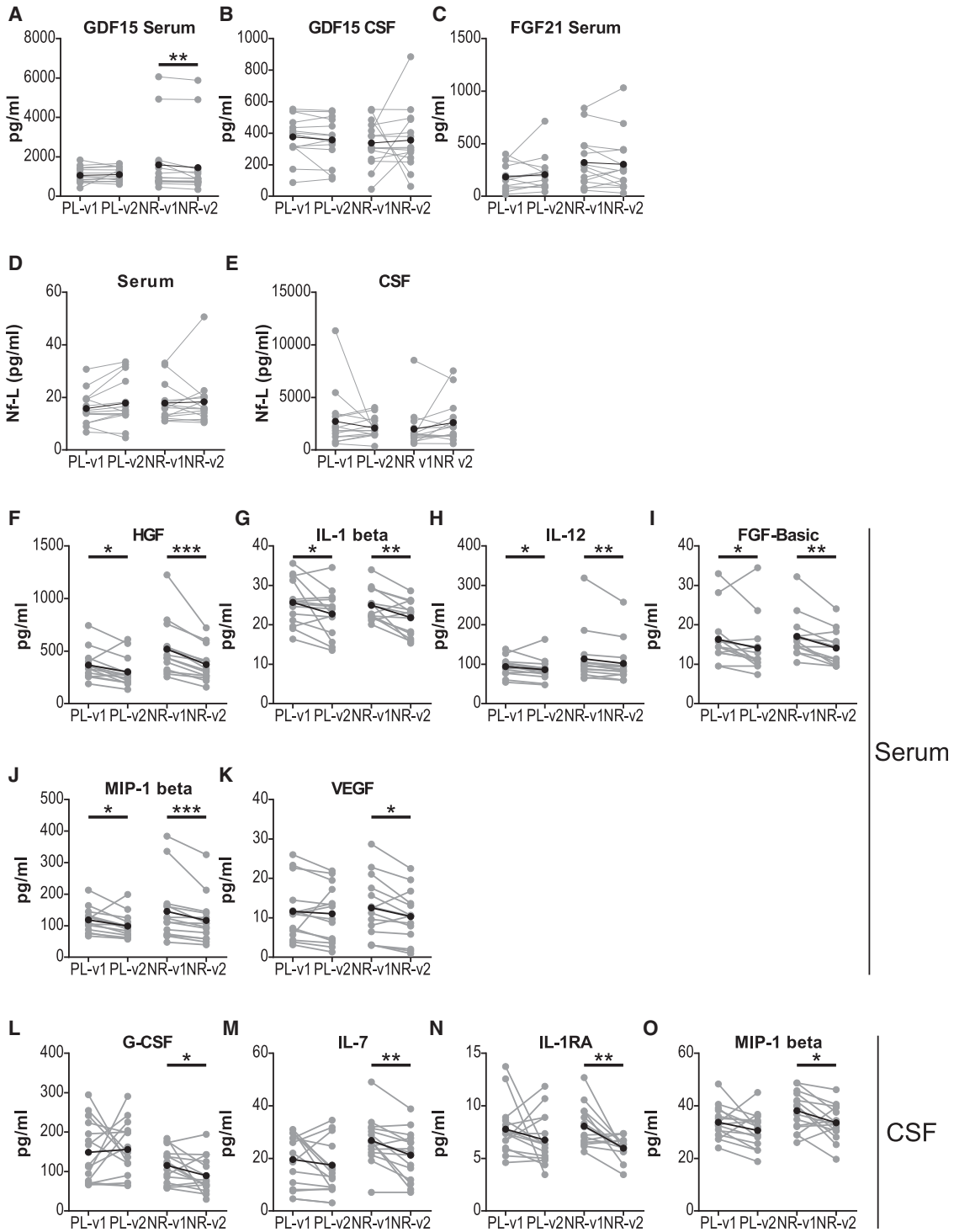

Figure 4. Serological markers affected by NR treatment

(A–C) Serological marker analysis in serum and CSF of PD patients in the placebo (PL) and NR-treated (NR) group before (V1) and after (V2) treatment. Data points show individual measurements (gray) and averages (black). Levels of GDF15 in serum (A) and CSF (B), and serum levels of FGF21 (C) are shown.

(D and E) Neurofilament light (Nf-L) chain levels in serum and CSF.

(F–O) Cytokine analysis in serum (F–K) and CSF (L–O). The plots show the cytokines that changed only, or with stronger significance, in the NR group.

*$p < 0.05$, **$p < 0.01$, ***$p < 0.001$ (Wilcoxon test).

Another metabolite of interest was acetyl-CoA, donor of acetyl-groups for acetylation reactions, including histone acetylation (Pietrocola et al., 2015). Higher NAD availability could lead to increased acetyl-CoA synthesis by promoting glucose and fatty acid catabolism. This could, in turn, exacerbate the histone hyperacetylation state observed in the PD brain (Park et al., 2016; Toker et al., 2021), further dysregulating gene expression. Our analyses detected no significant changes in acetyl-CoA or CoA levels upon NR supplementation. Finally, we monitored energy metabolites, such as ATP, ADP, AMP, as well as GTP and GDP. None of these showed a significant change upon NR supplementation.

The downstream metabolic impact of NR treatment was supported by the transcriptomic analyses in PBMC and muscle, which revealed effects in multiple disease-relevant pathways. Notably, NR was associated with upregulation of genes involved in mitochondrial respiration, antioxidant response, and protein degradation, including the proteasome and lysosome. Quantitative and functional respiratory deficiency (Fløngs et al., 2018; Schapira et al., 1989), increased oxidative damage (Dias et al., 2013; Jenner, 2003), and impaired proteasomal and lysosomal function (Lehtonen et al., 2019) have all been strongly implicated in the pathophysiology of PD. Therefore, these findings are encouraging, and they support a potential neuroprotective effect of NR in PD. Furthermore, our results indicate that NR may have anti-inflammatory action by decreasing the levels of inflammatory cytokines not only peripherally as previously shown in healthy aged individuals (Elhassan et al., 2019) but also in the central nervous system. Interestingly, almost all serum cytokines showing a significant decrease in the NR group also decreased in the placebo group, making the significance of these findings uncertain. In contrast, several CSF cytokines showed a significant decrease exclusively in the NR-treated group, suggesting a potential anti-inflammatory effect in the nervous system. Neuroinflammation has been implicated in the pathogenesis of PD, and it is considered a potential target for neuroprotection (Rocha et al., 2015).

Mitochondrial biomarker analyses revealed a mild, but significant, decrease of GDF15 in the serum, but not CSF, of NR recipients. This is in line with the observed transcriptomic upregulation of mitochondrial genes and could be indicative of improved mitochondrial function in our patients. Nf-L levels were not significantly affected by NR treatment in serum or CSF. However, Nf-L is only mildly elevated in PD (especially in early stages of the disease) compared with healthy controls and is better suited as a biomarker for monitoring disease progression over time (Mollenhauer et al., 2020). Therefore, also given the small sample size and short duration of our trial, the lack of Nf-L change is not surprising.

Conclusions

In conclusion, the study meets its primary outcome and shows that oral NR therapy increases brain NAD levels and impacts cerebral metabolism in PD. Furthermore, our findings suggest that NR may target multiple processes implicated in the pathophysiology of the disease by upregulating the expression of genes involved in mitochondrial respiration, oxidative damage response, lysosomal and proteasomal function, and downregulating inflammatory cytokines in the central nervous system. In addition, it is possible that NR may mitigate epigenomic dysregulation in PD by regulating histone acetylation. Genome-wide histone hyperacetylation and altered transcriptional regulation occur in the brain of individuals with PD (Toker et al., 2021). Increasing neuronal NAD levels would boost the activity of the NAD-dependent histone deacetylases of the sirtuin family, potentially ameliorating histone hyperacetylation in PD. Taken together, our findings nominate NR as a potential neuroprotective agent against PD, which warrants further investigation in a larger trial. To this end, we are currently conducting the phase II trial NOPARK (Clinicaltrials.gov: NCT03568968), aiming to assess whether NR can delay nigrostriatal degeneration and clinical disease progression in patients with early PD.

Limitations of study

The sample size of this trial was relatively small, although we had adequate power to robustly support the primary and most of the secondary and tertiary outcomes. The observed trend for clinical improvement among the NR recipients with increased cerebral NAD levels should be interpreted with caution due to the low number of subjects, short observation time, and high interindividual variability in MDS-UPDRS scores. While these observations are encouraging, only a phase II trial will provide conclusive clinical evidence on any disease-modifying effects of NR in PD. Although we were able to confidently detect and measure total cerebral NAD levels by ^{31}P-MRS, our analyses were limited by the strength of the magnet used in this study, as well as adhering to normal-mode specific absorption rate (SAR) levels, which did not allow us to confidently discriminate between the oxidized (NAD^+) and reduced (NADH) forms. A higher field strength or more effective decoupling by increasing SAR deposition limit may make discrimination possible (Lu et al., 2014; Peeters et al., 2019). More detailed analysis of the NAD^+/NADH redox ratio in the brain upon NR treatment would improve our knowledge about the metabolic impacts of NR in the brain. The transcriptomic analyses showed an NR-associated upregulation of genes involved in mitochondrial respiration. Establishing whether this leads to improved mitochondrial respiration would require the assessment of respiratory enzyme activities in the patients' tissue. Performing these analyses post hoc was not feasible in this trial due to the limited tissue sample availability.

STAR★METHODS

Detailed methods are provided in the online version of this paper and include the following:

- KEY RESOURCES TABLE
- RESOURCE AVAILABILITY
  - Lead contact
  - Materials availability
  - Data and code availability
- EXPERIMENTAL MODEL AND SUBJECT DETAILS
  - Participants and study design
  - Approval, registration, and patient consent
  - Randomization and masking
- METHOD DETAILS
  - Outcomes
  - Procedures

SUPPLEMENTAL INFORMATION

Supplemental information can be found online at https://doi.org/10.1016/j.cmet.2022.02.001.

ACKNOWLEDGMENTS

We are grateful to our study nurse, Marit Renså, and technical laboratory staff, Hanne Linda Nakkestad, Gry Hilde Nilsen, Dagny-Ann Sandnes, Kibret Yimer Mazengia, Wenche Hauge Eilifsen, and Kristin Paulsen Rye, for excellent technical assistance. We thank Prof. Kjell-Morten Myhr for the fruitful discussions and ChromaDex (Irvine, California) for providing the NR and placebo capsules. We also thank Anne Mathilde Kvammen, Research and Development Department, Haukeland University Hospital; Dr Ann Cathrine Kroksveen, Biobank Haukeland, Haukeland University Hospital; Dr Cecilie B. Rygh, Department of Radiology, Haukeland University Hospital; and Prof. Martin Biermann, Department of Nuclear Medicine, Haukeland University Hospital. We are grateful to the staff at the Department of Neurology, Department of Radiology and the PET-Center, Haukeland University Hospital, for providing essential personnel and infrastructure for the study. This work was supported by grants from The Research Council of Norway (288164), Bergen Research Foundation (BFS2017REK05), and the Western Norway Regional Health Authority (F-11470). The funder of the study had no role in study design, data collection, data analysis, data interpretation, or writing of the report.

AUTHOR CONTRIBUTIONS

Study conceptualization, C.T. and C.D.; design, C.T., B.B., and C.D.; clinical trial execution, B.B., K.H., G.O.S., O.-B.T., and C.T.; data collection, B.B., C.D., K.H., G.O.S., O.-B.T., T.S., N.B., V.S., K.V., L.S., J.D., R.G., and C.T.; data analyses and interpretation, B.B., C.D., F.R., Y.M., G.S.N., A.R.C., T.S., N.B., V.S., K.V., L.S., J.D., S.P., R.G., D.E., M.Z., and C.T.; drafting the manuscript, B.B., C.D., F.R., Y.M., G.S.N., A.R.C., T.S., S.P., D.E., M.Z., and C.T. All authors have read and approved the manuscript.

DECLARATION OF INTERESTS

C.T. and C.D. have filed a patent application relating to the use of NR in PD. All other authors declare no competing interests.

Received: July 15, 2021
Revised: November 17, 2021
Accepted: January 31, 2022
Published: March 1, 2022

REFERENCES

Akie, T.E., Liu, L., Nam, M., Lei, S., and Cooper, M.P. (2015). OXPHOS-mediated induction of NAD+ promotes complete oxidation of fatty acids and interdicts non-alcoholic fatty liver disease. PLoS One *10*, e0125617.

Andrews, S. (2010). FastQC: a quality control tool for high throughput sequence data (Babraham Bioinformatics).

Asanuma, K., Tang, C., Ma, Y., Dhawan, V., Mattis, P., Edwards, C., Kaplitt, M.G., Feigin, A., and Eidelberg, D. (2006). Network modulation in the treatment of Parkinson's disease. Brain *129*, 2667–2678.

Ashburner, M., Ball, C.A., Blake, J.A., Botstein, D., Butler, H., Cherry, J.M., Davis, A.P., Dolinski, K., Dwight, S.S., Eppig, J.T., et al. (2000). Gene ontology: tool for the unification of biology. The Gene Ontology Consortium. Nat. Genet. *25*, 25–29.

Athauda, D., and Foltynie, T. (2015). The ongoing pursuit of neuroprotective therapies in Parkinson disease. Nat. Rev. Neurol. *11*, 25–40.

Bieganowski, P., and Brenner, C. (2004). Discoveries of nicotinamide riboside as a nutrient and conserved NRK genes establish a Preiss-Handler independent route to NAD+ in fungi and humans. Cell *117*, 495–502.

Bloem, B.R., Okun, M.S., and Klein, C. (2021). Parkinson's disease. Lancet *397*, 2284–2303.

Boenzi, S., and Diodato, D. (2018). Biomarkers for mitochondrial energy metabolism diseases. Essays Biochem. *62*, 443–454.

Braidy, N., and Liu, Y. (2020). NAD+ therapy in age-related degenerative disorders: a benefit/risk analysis. Exp. Gerontol. *132*, 110831.

Brown, K.D., Maqsood, S., Huang, J.Y., Pan, Y., Harkcom, W., Li, W., Sauve, A., Verdin, E., and Jaffrey, S.R. (2014). Activation of SIRT3 by the NAD(+) precursor nicotinamide riboside protects from noise-induced hearing loss. Cell Metab. *20*, 1059–1068.

Brüggemann, N., and Klein, C. (1993). Parkin type of early-onset Parkinson disease. In GeneReviews, M.P. Adam, H.H. Ardinger, R.A. Pagon, S.E. Wallace, L.J. Bean, G. Mirzaa, and A. Amemiya, eds. (University of Washington).

Conze, D.B., Crespo-Barreto, J., and Kruger, C.L. (2016). Safety assessment of nicotinamide riboside, a form of vitamin B3. Hum. Exp. Toxicol. *35*, 1149–1160.

Conze, D., Brenner, C., and Kruger, C.L. (2019). Safety and metabolism of long-term administration of NIAGEN (nicotinamide riboside chloride) in a randomized, double-blind, placebo-controlled clinical trial of healthy overweight adults. Sci. Rep. *9*, 9772.

de Rijk, M.C., Launer, L.J., Berger, K., Breteler, M.M., Dartigues, J.F., Baldereschi, M., Fratiglioni, L., Lobo, A., Martinez-Lage, J., Trenkwalder, C., and Hofman, A. (2000). Prevalence of Parkinson's disease in Europe: a collaborative study of population-based cohorts. Neurologic Diseases in the Elderly Research Group. Neurology *54* (*Suppl 5*), S21–S23.

Deelchand, D.K., Nguyen, T.-M., Zhu, X.-H., Mochel, F., and Henry, P.-G. (2015). Quantification of in vivo 31P NMR brain spectra using LCModel. NMR Biomed. *28*, 633–641.

Dias, V., Junn, E., and Mouradian, M.M. (2013). The role of oxidative stress in Parkinson's disease. J. Parkinsons Dis. *3*, 461–491.

Dollerup, O.L., Christensen, B., Svart, M., Schmidt, M.S., Sulek, K., Ringgaard, S., Stødkilde-Jørgensen, H., Møller, N., Brenner, C., Treebak, J.T., and Jessen, N. (2018). A randomized placebo-controlled clinical trial of nicotinamide riboside in obese men: safety, insulin-sensitivity, and lipid-mobilizing effects. Am. J. Clin. Nutr. *108*, 343–353.

Edden, R.A., Puts, N.A., Harris, A.D., Barker, P.B., and Evans, C.J. (2014). Gannet: a batch-processing tool for the quantitative analysis of gamma-aminobutyric acid–edited MR spectroscopy spectra. J. Magn. Reson. Imaging *40*, 1445–1452.

Elhassan, Y.S., Kluckova, K., Fletcher, R.S., Schmidt, M.S., Garten, A., Doig, C.L., Cartwright, D.M., Oakey, L., Burley, C.V., Jenkinson, N., et al. (2019). Nicotinamide riboside augments the aged human skeletal muscle NAD+ metabolome and induces transcriptomic and anti-inflammatory signatures. Cell Rep. *28*, 1717–1728.e6.

Espay, A.J., Brundin, P., and Lang, A.E. (2017). Precision medicine for disease modification in Parkinson disease. Nat. Rev. Neurol. *13*, 119–126.

Fløynes, I.H., Fernandez-Vizarra, E., Lykouri, M., Brakedal, B., Skeie, G.O., Miletic, H., Lilleng, P.K., Alves, G., Tysnes, O.-B., Haugarvoll, K., et al. (2018). Neuronal complex I deficiency occurs throughout the Parkinson's disease brain, but is not associated with neurodegeneration or mitochondrial DNA damage. Acta Neuropathol. *135*, 409–425.

Gillis, J., Mistry, M., and Pavlidis, P. (2010). Gene function analysis in complex data sets using ErmineJ. Nat. Protoc. *5*, 1148–1159.

Gonzalez-Hunt, C.P., and Sanders, L.H. (2021). DNA damage and repair in Parkinson's disease: recent advances and new opportunities. J. Neurosci. Res. *99*, 180–189.

Gooch, C.L., Pracht, E., and Borenstein, A.R. (2017). The burden of neurological disease in the United States: a summary report and call to action. Ann. Neurol. *81*, 479–484.

Guarino, M., and Dufour, J.-F. (2019). Nicotinamide and NAFLD: is there nothing new under the sun? Metabolites *9*, 180.

Habeck, C., Krakauer, J.W., Ghez, C., Sackeim, H.A., Eidelberg, D., Stern, Y., and Moeller, J.R. (2005). A new approach to spatial covariance modeling of functional brain imaging data: ordinal trend analysis. Neural Comput. *17*, 1602–1645.

Habeck, C., and Stern, Y.; Alzheimer's Disease Neuroimaging Initiative (2010). Multivariate data analysis for neuroimaging data: overview and application to Alzheimer's disease. Cell Biochem. Biophys. *58*, 53–67.

Han, S., Du, Z., Liu, K., and Gong, S. (2020). Nicotinamide riboside protects noise-induced hearing loss by recovering the hair cell ribbon synapses. Neurosci. Lett. *725*, 134910.

Harlan, B.A., Killoy, K.M., Pehar, M., Liu, L., Auwerx, J., and Vargas, M.R. (2020). Evaluation of the NAD+ biosynthetic pathway in ALS patients and effect of modulating NAD+ levels in hSOD1-linked ALS mouse models. Exp. Neurol. *327*, 113219.

Hattori, N., Tanaka, M., Ozawa, T., and Mizuno, Y. (1991). Immunohistochemical studies on complexes I, II, III, and IV of mitochondria in Parkinson's disease. Ann. Neurol. *30*, 563–571.

Hirsch, E.C., and Hunot, S. (2009). Neuroinflammation in Parkinson's disease: a target for neuroprotection? Lancet Neurol. *8*, 382–397.

Jadavji, N.M., Wieske, F., Dirnagl, U., and Winter, C. (2015). Methylenetetrahydrofolate reductase deficiency alters levels of glutamate and γ-aminobutyric acid in brain tissue. Mol. Genet. Metab. Rep. *3*, 1–4.

Jenner, P. (2003). Oxidative stress in Parkinson's disease. Ann. Neurol. *53* (*Suppl 3*), S26–S38.

Johnson, S., and Imai, S.-I. (2018). NAD+ biosynthesis, aging, and disease. F1000Res. *7*, 132.

Kalia, L.V., and Lang, A.E. (2015). Parkinson's disease. Lancet *386*, 896–912.

Katsyuba, E., Romani, M., Hofer, D., and Auwerx, J. (2020). NAD+ homeostasis in health and disease. Nat. Metab. *2*, 9–31.

Ko, J.H., Feigin, A., Mattis, P.J., Tang, C.C., Ma, Y., Dhawan, V., During, M.J., Kaplitt, M.G., and Eidelberg, D. (2014). Network modulation following sham surgery in Parkinson's disease. J. Clin. Invest. *124*, 3656–3666.

Lamb, D.A., Moore, J.H., Mesquita, P.H.C., Smith, M.A., Vann, C.G., Osburn, S.C., Fox, C.D., Lopez, H.L., Ziegenfuss, T.N., Huggins, K.W., et al. (2020). Resistance training increases muscle NAD+ and NADH concentrations as well as NAMPT protein levels and global sirtuin activity in middle-aged, overweight, untrained individuals. Aging (Albany, NY) *12*, 9447–9460.

Lautrup, S., Sinclair, D.A., Mattson, M.P., and Fang, E.F. (2019). NAD+ in brain aging and neurodegenerative disorders. Cell Metab. *30*, 630–655.

Lehtonen, J.M., Forsström, S., Bottani, E., Viscomi, C., Baris, O.R., Isoniemi, H., Höckerstedt, K., Österlund, P., Hurme, M., Jylhävä, J., et al. (2016). FGF21 is a biomarker for mitochondrial translation and mtDNA maintenance disorders. Neurology *87*, 2290–2299.

Lehtonen, Š., Sonninen, T.-M., Wojciechowski, S., Goldsteins, G., and Koistinaho, J. (2019). Dysfunction of cellular proteostasis in Parkinson's disease. Front. Neurosci. *13*, 457.

Love, M.I., Huber, W., and Anders, S. (2014). Moderated estimation of fold change and dispersion for RNA-seq data with DESeq2. Genome Biol. *15*, 550.

Lozza, C., Baron, J.-C., Eidelberg, D., Mentis, M.J., Carbon, M., and Marié, R.M. (2004). Executive processes in Parkinson's disease: FDG-PET and network analysis. Hum. Brain Mapp. *22*, 236–245.

Lu, M., Zhu, X.-H., Zhang, Y., and Chen, W. (2014). Intracellular redox state revealed by in vivo (31) P MRS measurement of NAD(+) and NADH contents in brains. Magn. Reson. Med. *71*, 1959–1972.

Martens, C.R., Denman, B.A., Mazzo, M.R., Armstrong, M.L., Reisdorph, N., McQueen, M.B., Chonchol, M., and Seals, D.R. (2018). Chronic nicotinamide riboside supplementation is well-tolerated and elevates NAD+ in healthy middle-aged and older adults. Nat. Commun. *9*, 1286.

Mollenhauer, B., Dakna, M., Kruse, N., Galasko, D., Foroud, T., Zetterberg, H., Schade, S., Gera, R.G., Wang, W., Gao, F., et al. (2020). Validation of serum neurofilament light chain as a biomarker of Parkinson's disease progression. Mov. Disord. *35*, 1999–2008.

Monaco, G., Lee, B., Xu, W., Mustafah, S., Hwang, Y.Y., Carré, C., Burdin, N., Visan, L., Ceccarelli, M., Poidinger, M., et al. (2019). RNA-seq signatures normalized by mRNA abundance allow absolute deconvolution of human immune cell types. Cell Rep. *26*, 1627–1640.e7.

Mukherjee, S., Chellappa, K., Moffitt, A., Ndungu, J., Dellinger, R.W., Davis, J.G., Agarwal, B., and Baur, J.A. (2017). Nicotinamide adenine dinucleotide biosynthesis promotes liver regeneration. Hepatology *65*, 616–630.

Mure, H., Hirano, S., Tang, C.C., Isaias, I.U., Antonini, A., Ma, Y., Dhawan, V., and Eidelberg, D. (2011). Parkinson's disease tremor-related metabolic network: characterization, progression, and treatment effects. Neuroimage *54*, 1244–1253.

Mure, H., Tang, C.C., Argyelan, M., Ghilardi, M.-F., Kaplitt, M.G., Dhawan, V., and Eidelberg, D. (2012). Improved sequence learning with subthalamic nucleus deep brain stimulation: evidence for treatment-specific network modulation. J. Neurosci. *32*, 2804–2813.

Near, J., Edden, R., Evans, C.J., Paquin, R., Harris, A., and Jezzard, P. (2015). Frequency and phase drift correction of magnetic resonance spectroscopy data by spectral registration in the time domain. Magn. Reson. Med. *73*, 44–50.

Niethammer, M., and Eidelberg, D. (2012). Metabolic brain networks in translational neurology: concepts and applications. Ann. Neurol. *72*, 635–647.

Niethammer, M., Tang, C.C., Vo, A., Nguyen, N., Spetsieris, P., Dhawan, V., Ma, Y., Small, M., Feigin, A., During, M.J., et al. (2018). Gene therapy reduces Parkinson's disease symptoms by reorganizing functional brain connectivity. Sci. Transl. Med. *10*, eaau0713.

Okur, M.N., Mao, B., Kimura, R., Haraczy, S., Fitzgerald, T., Edwards-Hollingsworth, K., Tian, J., Osmani, W., Croteau, D.L., Kelley, M.W., and Bohr, V.A. (2020). Short-term NAD+ supplementation prevents hearing loss in mouse models of Cockayne syndrome. NPJ Aging Mech. Dis. *6*, 1.

Park, G., Tan, J., Garcia, G., Kang, Y., Salvesen, G., and Zhang, Z. (2016). Regulation of histone acetylation by autophagy in Parkinson disease. J. Biol. Chem. *291*, 3531–3540.

Patro, R., Duggal, G., Love, M.I., Irizarry, R.A., and Kingsford, C. (2017). Salmon provides fast and bias-aware quantification of transcript expression. Nat. Methods *14*, 417–419.

Peeters, T.H., van Uden, M.J., Rijpma, A., Scheenen, T.W., and Heerschap, A. (2019). 3D 31P MR spectroscopic imaging of the human brain at 3 T with a 31P receive array: an assessment of 1H decoupling, T1 relaxation times, 1H–31P nuclear Overhauser effects and NAD+. NMR Biomed. *34*, e4169.

Peng, S., Ma, Y., Spetsieris, P.G., Mattis, P., Feigin, A., Dhawan, V., and Eidelberg, D. (2014). Characterization of disease-related covariance topographies with SSMPCA toolbox: effects of spatial normalization and PET scanners. Hum. Brain Mapp. *35*, 1801–1814.

Petrillo, S., Schirinzi, T., Di Lazzaro, G.D., D'Amico, J., Colona, V.L., Bertini, E., Pierantozzi, M., Mari, L., Mercuri, N.B., Piemonte, F., and Pisani, A. (2020). Systemic activation of Nrf2 pathway in Parkinson's disease. Mov. Disord. *35*, 180–184.

Pietrocola, F., Galluzzi, L., Bravo-San Pedro, J.M., Madeo, F., and Kroemer, G. (2015). Acetyl coenzyme A: a central metabolite and second messenger. Cell Metab. *21*, 805–821.

Postuma, R.B., Berg, D., Stern, M., Poewe, W., Olanow, C.W., Oertel, W., Obeso, J., Marek, K., Litvan, I., Lang, A.E., et al. (2015). MDS clinical diagnostic criteria for Parkinson's disease. Mov. Disord. *30*, 1591–1601.

Purvis, L.A.B., Clarke, W.T., Biasiolli, L., Valkovič, L., Robson, M.D., and Rodgers, C.T. (2017). OXSA: an open-source magnetic resonance spectroscopy analysis toolbox in MATLAB. PLoS One *12*, e0185356.

Ren, J., Shang, T., Sherry, A.D., and Malloy, C.R. (2018). Unveiling a hidden 31P signal coresonating with extracellular inorganic phosphate by outer-volume-suppression and localized 31P MRS in the human brain at 7T. Magn. Reson. Med. *80*, 1289–1297.

Rocha, N.P., de Miranda, A.S., and Teixeira, A.L. (2015). Insights into neuroinflammation in Parkinson's disease: from biomarkers to anti-inflammatory based therapies. BioMed Res. Int. *2015*, 628192.

Schapira, A.H., Cooper, J.M., Dexter, D., Jenner, P., Clark, J.B., and Marsden, C.D. (1989). Mitochondrial complex I deficiency in Parkinson's disease. Lancet *1*, 1269.

Schindlbeck, K.A., and Eidelberg, D. (2018). Network imaging biomarkers: insights and clinical applications in Parkinson's disease. Lancet Neurol. *17*, 629–640.

Schöndorf, D.C., Ivanyuk, D., Baden, P., Sanchez-Martinez, A., De Cicco, S., Yu, C., Giunta, I., Schwarz, L.K., Di Napoli, G., Panagiotakopoulou, V., et al. (2018). The NAD+ precursor nicotinamide riboside rescues mitochondrial defects and neuronal loss in iPSC and fly models of Parkinson's disease. Cell Rep. *23*, 2976–2988.

Soneson, C., Love, M.I., and Robinson, M.D. (2015). Differential analyses for RNA-seq: transcript-level estimates improve gene-level inferences. F1000Res. *4*, 1521.

Sorrentino, V., Romani, M., Mouchiroud, L., Beck, J.S., Zhang, H., D'Amico, D., Moullan, N., Potenza, F., Schmid, A.W., Rietsch, S., et al. (2017). Enhancing mitochondrial proteostasis reduces amyloid-β proteotoxicity. Nature *552*, 187–193.

Spetsieris, P., Ma, Y., Peng, S., Ko, J.H., Dhawan, V., Tang, C.C., and Eidelberg, D. (2013). Identification of disease-related spatial covariance patterns using neuroimaging data. J. Vis. Exp. 50319.

Starcevic, M., and Dell'Angelica, E.C. (2004). Identification of snapin and three novel proteins (BLOS1, BLOS2, and BLOS3/reduced pigmentation) as subunits of biogenesis of lysosome-related organelles complex-1 (BLOC-1). J. Biol. Chem. *279*, 28393–28401.

Tang, C.C., Feigin, A., Ma, Y., Habeck, C., Paulsen, J.S., Leenders, K.L., Teune, L.K., van Oostrom, J.C., Guttman, M., Dhawan, V., and Eidelberg, D. (2013). Metabolic network as a progression biomarker of premanifest Huntington's disease. J. Clin. Invest. *123*, 4076–4088.

Teune, L.K., Renken, R.J., Mudali, D., De Jong, B.M., Dierckx, R.A., Roerdink, J.B.T.M., and Leenders, K.L. (2013). Validation of parkinsonian disease-related metabolic brain patterns. Mov. Disord. *28*, 547–551.

Toker, L., Tran, G.T., Sundaresan, J., Tysnes, O.-B., Alves, G., Haugarvoll, K., Nido, G.S., Dölle, C., and Tzoulis, C. (2021). Genome-wide histone acetylation analysis reveals altered transcriptional regulation in the Parkinson's disease brain. Mol. Neurodegener. *16*, 31.

Trammell, S.A., Schmidt, M.S., Weidemann, B.J., Redpath, P., Jaksch, F., Dellinger, R.W., Li, Z., Abel, E.D., Migaud, M.E., and Brenner, C. (2016). Nicotinamide riboside is uniquely and orally bioavailable in mice and humans. Nat. Commun. *7*, 12948.

Wu, P., Wang, J., Peng, S., Ma, Y., Zhang, H., Guan, Y., and Zuo, C. (2013). Metabolic brain network in the Chinese patients with Parkinson's disease based on 18F-FDG PET imaging. Parkinsonism Relat. Disord. *19*, 622–627.

Xie, X., Gao, Y., Zeng, M., Wang, Y., Wei, T.-F., Lu, Y.-B., and Zhang, W.-P. (2019). Nicotinamide ribose ameliorates cognitive impairment of aged and Alzheimer's disease model mice. Metab. Brain Dis. *34*, 353–366.

STAR★METHODS

KEY RESOURCES TABLE

REAGENT or RESOURCE	SOURCE	IDENTIFIER
Critical commercial assays		
Simoa NF-light Advantage (SR-X) Kit	Quanterix	Cat#103400
GDF-15/MIC-1 Human ELISA	BioVendor	Cat# RD191135200R
Fibroblast Growth Factor 21 Human ELISA	BioVendor	RD191108200R
Human Cytokine Magnetic 35-plex panel	Invitrogen	LHC6005M
Deposited data		
Raw sequencing counts	This paper	https://git.app.uib.no/neuromics/nadpark
Software and algorithms		
fastQC v0.11.9	Babraham Institute	http://www.bioinformatics.babraham.ac.uk/projects/fastqc
Salmon v1.3.0	Patro et al., 2017	https://github.com/COMBINE-lab/salmon
R v4.0.4	R core team	https://www.R-project.org/
DESeq2 R package v1.22.2	Love et al., 2014	https://bioconductor.org/packages/release/bioc/html/DESeq2.html
tximport R package v1.8.0	Soneson et al., 2015	https://bioconductor.org/packages/release/bioc/html/tximport.html
ermineR R package v1.0.1	Gillis et al., 2010	https://github.com/PavlidisLab/ermineR
ABIS algorithm	Monaco et al., 2019	https://github.com/giannimonaco/ABIS
GraphPad Prism v 6.07	GraphPad Software	N/A
SPSS	SPSS, Chicago, IL	N/A
3T Siemens Biograph mMR scanner, software version VE11P-SP03	Siemens, Munich, Germany	N/A
in-house Scan Analysis and Visualization (ScAnVP) software	N/A	http://feinsteinneuroscience.org
Statistical Parametric Mapping (SPM8) software	Wellcome Centre for Human Neuroimaging, London, UK	http://fil.ion.ucl.ac.uk/spm
Spectral Registration implementation from Gannet 3.0	Edden et al., 2014; Near et al., 2015	N/A
Matlab 9.5	MathWorks, Natick, MA	N/A
OXSA toolbox	Purvis et al., 2017	https://github.com/oxsatoolbox/oxsa
Thermo Xcalibur software	ThermoFisher Scientific	N/A
Other		
RNA-sequencing analyses and resources	This paper	https://git.app.uib.no/neuromics/nadpark

RESOURCE AVAILABILITY

Lead contact

Further information and requests for resources and reagents should be directed to and will be fulfilled by the lead contact, Charalampos Tzoulis (charalampos.tzoulis@uib.no).

Materials availability

This study did not generate new unique reagents.

Data and code availability

The data associated with Figures 1, 2, 3, 4, S1, and S3–S6 are available in the Data S1. The datasets required to reproduce the results of the RNA-seq analyses, including pre-processed raw counts and code for all downstream analyses, are publicly available in the Neuromics Group repository, https://git.app.uib.no/neuromics/nadpark.

All original code has been deposited in the Neuromics Group repository, https://git.app.uib.no/neuromics/nadpark and is publicly available as of the date of publication.
Any additional information required to reanalyze the data reported in this paper is available from the lead contact upon request.

EXPERIMENTAL MODEL AND SUBJECT DETAILS

Participants and study design

A single-center, double-blinded, randomized, placebo-controlled phase I trial of oral NR supplementation in newly diagnosed, treatment naïve patients with PD, was conducted at the Department of Neurology, Haukeland University Hospital, from January, 25th, 2019 to February, 12th, 2020. Inclusion criteria were: (i) a new clinical diagnosis of PD, (ii) drug naïve state with respect to dopaminergic treatment, (iii) clinical diagnosis of PD, according to the Movement Disorder Society Clinical Diagnostic Criteria (Postuma et al., 2015). Exclusion Criteria were: (i) [^{123}I]FP-CIT single photon emission CT (DaTscan) without evidence of nigrostriatal degeneration, (ii) Magnetic Resonance Imaging (MRI) suggestive of atypical parkinsonism, (iii) dementia or other neurological disorder at baseline visit, and (iv) metabolic, neoplastic, or other physically or mentally debilitating disorder at baseline visit. One participant (patient 1-027) had disease onset below the age of 40 years. Due to the early onset, this patient underwent genetic investigation with whole-exome sequencing and SNP-chip based genome-wide copy number variation analysis. These analyses excluded pathogenic mutations in PD-related genes, including *PRKN*, *PINK1* and *PARK7*, mutations in which are known to cause early onset disease (Brüggemann et al., Klein, 1993). Patient recruitment, inclusion, and follow-up was carried out by a GCP certified investigator. The demographic information of the participants is provided in Tables 1 and S2. A CONSORT flow diagram for the trial is provided in Figure S1.

Approval, registration, and patient consent

The research protocol was approved by the Regional Committee for Medical and Health Research Ethics, Western Norway (2018/597). Patients were identified and recruited at the Department of Neurology, Haukeland University Hospital, Norway. Written and informed consent was obtained from all participants from investigators in NADPARK. This study followed Good Clinical Practice guidelines. The trial is registered at Clinicaltrials.gov, identifier: NCT03816020.

Randomization and masking

Thirty PD patients were randomly assigned (Block size 6, allocation 1:1) to 500 mg NR or placebo twice per day, 12 hours apart, using the electronic Case Report Form (https://www.viedoc.com/). The drug containers were sequentially marked by an independent third party, the Research and Development department, Haukeland University hospital. The NR (Niagen) and placebo were provided by ChromaDex, USA. Each NR capsule contained 250 mg of NR. Placebo capsules contained only microcrystalline cellulose. The vials and capsules containing NR and placebo were identical in shape, color, and smell. Study drug compliance was calculated from counting returned number of study capsules and self-reporting. The Center for Clinical Research, Haukeland University Hospital provided allocation sequence, packing and labeling of drugs in participant-specific kits. Participants, examining physicians, medical- and research personnel were blinded for the duration of the trial. Sample size was determined by comparing previous literature with respect to the primary objective.

METHOD DETAILS

Outcomes

The primary objective of the study was to assess penetration and metabolic responses of the brain, by determining whether oral NR treatment increases cerebral NAD and impacts the neurometabolic profile of patients with PD, based on neuroimaging measures (FDG-PET, ^{31}P-MRS). Secondary objectives were to determine if NR improves clinical symptoms measured using MDS-UPDRS and whether it augments the NAD metabolome in peripheral tissue of PD patients. Additional secondary measures included frequency of adverse events, changes in vital signs, and clinical laboratory values. Exploratory outcome measures assessed the effect of NR on gene-expression in PBMCs and muscle (RNA-seq), blood and CSF biomarkers of neuronal damage, mitochondrial function, and inflammation.

Procedures

At screening for trial entry, candidates underwent physical and neurological examination, brain MRI, and DaTscan. Eligible patients who entered the trial were assessed at baseline (visit 1, V1) and after four weeks of exposure to either NR or placebo (visit 2, V2). At both visits, patients underwent physical and neurological examination, including assessment by the Movement Disorder Society Unified Parkinson's Disease Rating Scale section I-IV (MDS-UPDRS), and biological sampling. MR-PET was performed within one week prior to visit 1, and at visit 2. All participants remained naive for antiparkinson drugs for the duration of the trial. All clinical assessments were performed by a blinded movement disorders expert. Each patient was examined by the same neurologist at both visits. Methodological details on each procedure are provided below. Safety was monitored through routine clinical blood tests (Methods S1) and registration of adverse events. Adverse events (AE) were recorded and scored by the investigative physician. Severity was scored according to severity grading defined by Common Terminology Criteria for Adverse Events v5.0 (CTCAE) as (1) mild, (2)

moderate, (3) severe, (4) life-threatening or (5) death. The AE relation to the study drug was scored as (1) unrelated, (2) unlikely, (3) possible, (4) probable or (5) definitely.

Biological sampling

Biological material was collected at both visits, following a minimum 6-hour fasting and within 6 hours after study drug intake for visit 2. Sampling included whole blood, serum, peripheral blood mononuclear cells (PBMCs), cerebrospinal fluid (CSF) and muscle biopsy. Lumbar puncture was performed according to standard clinical procedures to collect 10 ml CSF (Methods S1). Needle biopsy of the vastus lateralis muscle was performed using a Bard Magnum biopsy gun (BD©, United States) and 12Gx10cm biopsy needles. Muscle biopsies were immediately dissected to remove any non-muscle tissue (e.g., fat or fascia) and snap-frozen in liquid nitrogen. Detailed protocols on sample collection and storage are provided in the NADPARK laboratory protocol (Methods S1).

Magnetic resonance imaging and spectroscopy (MRI/S)

MRI/S was conducted on a 3T Biograph mMR MR-PET scanner (Siemens Healthcare, Germany). Phosphorous MRS (^{31}P-MRS) was performed on a double-resonant transmit/receive ^{1}H/^{31}P volume head-coil (Rapid Biomedical, Germany).

An anatomical T1-weighted image with the following sequence parameters was acquired to aid positioning of the ^{31}P-imaging slab: MPRAGE 3D T1-weighted sagittal volume, TE/TR/TI = 2.26 ms /2.4 s /900 ms, acquisition matrix = 256 × 256 × 192, FOV = 256 × 256 x 192 mm3, 200 Hz/px readout bandwidth, flip angle = 8 degrees and total acquisition duration of 5.6 minutes.

^{31}P spectroscopy data were acquired using a 3D chemical shift imaging (CSI) FID sequence with WALTZ4 1H decoupling and continuous wave nuclear Overhauser effect (NOE) enhancement (Peeters et al., 2019). A CSI grid with an 8 x 8 matrix and nominal voxel size of 30 x 30 x 80 mm^3, 1024 samples, readout length = 512 ms, 1000 Hz bandwidth, field of view (FOV) = 240 x 240 x 80 mm^3, TE/TR = 2.3 ms / 3.0 s, 10 averages, flip angle = 90 degrees and total acquisition duration of 14.5 minutes, were used. Rectangular NOE pulses of 10 ms length, interpulse delay 1ms, train length 10 prior and WALTZ4 decoupling (2ms pulses, 180 deg. flip angle) were applied prior to ^{31}P-excitation and during the first half of the acquisition window respectively. The FOV was centered on the brain midline and aligned parallel to the anterior and posterior commissure.

The ^{31}P-MRS data from three individuals (one in the placebo group and two in the NR group) were lost due to technical error. Thus, ^{31}P-MRS data from a total of 27 individuals (14 the placebo group and 13 in the NR group) were available for downstream analyses. Spectra from the occipital region were aligned using an adaption of the Spectral Registration implementation from Gannet 3.0 (Edden et al., 2014; Near et al., 2015), subject to thresholding on SNR (>=3) to eliminate the majority of out-of-brain voxels. Voxels were averaged before being processed in Matlab 9.5 (the MathWorks, Natick, MA) using the OXSA (Purvis et al., 2017) toolbox utilizing first order phase correction and fitting with AMARES. Custom prior information was created based on literature values for membrane phospholipids (MP), glycerophosphocholine (GPC), glycerophosphoethanolamine (GPE), inorganic phosphate (Pi), phosphocoline (PC), phosphoethanolamine (PE) as well as alpha-, beta- and gamma resonances of adenosine triphosphate (ATP-α, -β, and –γ, respectively) in reference to the phosphocreatine (PCr) peak (Deelchand et al., 2015; Peeters et al., 2019; Ren et al., 2018). Additional information for the properties of nicotinamide adenine dinucleotide (NAD) was added based on the framework developed by Lu et al. (2014) by calculating field-strength dependent chemical shift differences, relative amplitudes and frequency separations for oxidized and reduced NAD (NAD$^+$ and NADH, respectively). Linewidths were fixed to be equal for NAD$^+$, NADH and ATP-α. At 3T, and to comply with normal-mode specific absorption rate (SAR) restrictions, peak separation for NAD$^+$ and NADH was limited and therefore only combined values of total NAD (NAD$^+$ and NADH together) are reported.

Positron emission tomography (PET)

PET-MRI imaging was performed with a 3T Siemens Biograph mMR scanner, software version VE11P-SP03. Subjects were administered 200 MBq of ^{18}Fluoro-deoxyglucose (FDG) before being positioned in the scanner. After ^{31}P-MRS spectra had been acquired, an 8-channel Siemens mMR Head coil was used for further MR imaging, which was performed simultaneously with FDG-PET. In all subjects, PET acquisition began 25 to 30 minutes after the injection of FDG and lasted 30 minutes. The resulting emission data were reconstructed using Siemens HD-PET algorithm with Siemens HiRes Brain MRAC, with voxel size of 2.3 x 2.3 x 5.0 mm^3. PET images were anonymized and archived as DICOM files with a matrix size of 344 × 344 × 127 and an isotropic voxel size of 2.09 × 2.09 × 2.03 mm^3.

FDG-PET scans were transferred electronically to the Center for Neurosciences at The Feinstein Institutes for Medical Research (Manhasset, NY, USA) and analyzed using automated computing pipelines implemented in MATLAB 7.5 (MathWorks, Natick, MA) using in-house Scan Analysis and Visualization (ScAnVP) software (available at http://feinsteinneuroscience.org). Images were first pre-processed using Statistical Parametric Mapping (SPM8) software (http://fil.ion.ucl.ac.uk/spm; Wellcome Centre for Human Neuroimaging, London, UK). Of the 30 participants, the baseline scan of one subject in the NR group was excluded on technical grounds. Thus, a total of 29 scans (14 in the NR group and 15 in the placebo group) were available for downstream analyses (Table S2). In these 29 subjects, FDG-PET scans acquired at visit 1 and visit 2 were aligned to produce a mean image, which was spatially normalized in standard Montreal Neurological Institute (MNI) anatomic space along with the individual scans from each time point. The normalized images were then smoothed with a 10-mm Gaussian filter in three dimensions to enhance the signal to noise ratio.

For the PET-analyses, the subjects in the NR group were classified based on their cerebral NAD-response, measured by ^{31}P-MRS. Subjects showing increased cerebral NAD levels at visit 2 were termed ''MRS-responders'', whereas subjects showing no increase in cerebral NAD were termed ''MRS non-responders''.

To identify an NR-related metabolic pattern (NRRP), we analyzed paired metabolic scan data from the 10 MRS responders in the NR group (Table S3) using ordinal trends/canonical variates analysis (OrT/CVA), a supervised form of principal component analysis (PCA) (Habeck et al., 2005). This multivariate approach is designed to detect and quantify regional covariance patterns

(i.e., metabolic networks) for which expression values (i.e., subject scores) increase or decrease with treatment in all or most of the subjects (Ko et al., 2014; Mure et al., 2011, 2012; Niethammer et al., 2018; Tang et al., 2013). The significance of the resulting OrT/CVA topographies was assessed using nonparametric tests, i.e., permutation testing of the subject scores to show that the observed ordinal trend did not occur by chance. Likewise, the reliability of the voxel loadings (i.e., region weights) on the resulting network topography was assessed using bootstrap resampling procedures (Habeck and Stern, 2010; Mure et al., 2011).

In this study, we restricted the analysis to the top six PC patterns, which together accounted for greater than 75% of the subject × voxel variance in the longitudinal data. Expression values for these PCs were entered singly and in all possible linear combinations to identify significant monotonic trends in the individual subject data, i.e., consistent increases (or decreases) in pattern expression across the subjects with few if any violations ($p < 0.05$; permutation test, 1000 iterations). The resulting coefficients were applied to the corresponding PC patterns to construct the NR-related topography. For the NRRP to be significant, we required that voxel weights have low dispersion (inverse coefficient of variation (ICV) $|z| > 1.96$, $p<0.05$; bootstrap resampling (1,000 iterations), indicating that regional loadings were not driven by outliers). The current analysis was performed within the population gray matter brain mask defined by the FDG-PET scans. To standardize NRRP subject scores, we computed expression values for this pattern in an age-matched group of 22 healthy volunteers (11M/11F; age 62.9 ± 8.6 years) scanned at the Feinstein Institutes. Values in all trial participants (NR and placebo) were standardized (*z*-scored) with respect to these scans (Peng et al., 2014; Spetsieris et al., 2013).

To further examine the effect of NR therapy on metabolic network organization, we compared the NRRP to a specific PD-related metabolic pattern (PDRP) that has been extensively validated in prior studies (Schindlbeck and Eidelberg, 2018). PDRP expression levels (subject scores) were computed in all trial participants. These values were correlated with corresponding NRRP subject scores and UPDRS motor ratings in each condition. Correlations were likewise computed between the changes in these measures in the two groups.

RNA sequencing

For all subjects at both visits, total RNA was extracted from muscle biopsy tissue and PBMC homogenate using RNeasy plus mini kit (Qiagen) with on-column DNase treatment according to manufacturer's protocol. The final elution was made in 45 μl of dH2O. The concentration and integrity of the total RNA were estimated by Ribogreen assay (Thermo Fisher Scientific), and Fragment Analyzer (Advanced Analytical), respectively, and 10 ng of total RNA was used for downstream RNA-seq applications using the SMARTer Stranded Total RNA-Seq Kit v2 - Pico Input Mammalian Kit (IlluminaTakara Bio USA, Mountian View, CA) as per manufacturer's recommended protocol. Library quantity was assessed by Picogreen Assay (Thermo Fisher Scientific), and the library quality was estimated by utilizing a DNA High Sense chip on a Caliper Gx (Perkin Elmer). Accurate quantification of the final libraries for sequencing applications was determined using the qPCR-based KAPA Biosystems Library Quantification kit (Kapa Biosystems). Each library pooled equimolar prior to clustering. One hundred bp paired-end sequencing was performed on an Illumina NovaSeq S4 sequencer (Illumina). Two subjects were discarded from the PBMC samples and two from the muscle samples due to either insufficient tissue quantity/lack of sample, or being outliers in expression (see Table S2). RNA quality, as measured by the RNA integrity number (RIN), was satisfactory (mean = 7.6±1.1, range = 3.1-9.1 for PBMC samples; mean = 9.1±1.3, range = 5-10 for muscle), and was not significantly associated with visit or treatment (PBMC treatment∼RIN, $p = 0.47$; PBMC visit∼RIN, $p = 0.37$; muscle treatment∼RIN, $p = 0.21$; muscle visit∼RIN, $p = 0.99$, F-test).

FASTQ files were assessed using fastQC version 0.11.9 (Andrews, 2010). Quantification at the transcript level was calculated using Salmon version 1.3.0 (Patro et al., 2017) with fragment-level GC bias correction against the GENCODE version 35, with the whole genome as decoy sequence. Transcript-level quantification was collapsed onto gene-level using the tximport R package version 1.8.0 (Soneson et al., 2015). Genes in non-canonical chromosomes and scaffolds and transcripts encoded by the mitochondrial genome were filtered out, together with non-protein-coding genes. Low-expressed genes were likewise removed from downstream analyses (expression below 10 reads for 75% of the samples). PBMC and muscle datasets were analyzed independently. For PBMC samples, cell type composition was assessed employing ABIS (Monaco et al., 2019). Differential gene expression was performed using the DESeq2 R package version 1.22.2 (Love et al., 2014). The generalized linear model formula accounted for both interindividual variability between subjects and the normal course of the experiment (baseline for each subject and baseline for the time-course). Multiple hypothesis testing was performed with the default automatic filtering of DESeq2 followed by false discovery rate (FDR) calculation by the Benjamini-Hochberg procedure. Functional enrichment of both over- and under-expressed genes was carried out by ranking genes according to their p-value (accounting for the direction of change) and employing the gene score resampling method implemented in the ermineR package version 1.0.1, an R wrapper package for ermineJ (Gillis et al., 2010) with the complete Gene Ontology (GO) database annotation (Ashburner et al., 2000) to thus obtain lists of up- and down-regulated pathways for each dataset. Complete RNA-seq analyses are available at https://git.app.uib.no/neuromics/nadpark.

Metabolomic analysis

Muscle and PBMCs metabolomics

Standard substances of all the targeted compounds were used to prepare stock standard solutions and these solutions were mixed and diluted to make serially diluted standard solutions in an internal standard solution containing 11 isotope-labeled compounds (NAD-13C5, NADH-d5, nicotinamide riboside-d4, nicotinic-d4 acid, nicotinic acid-d4 riboside, AMP-15N5, ATP-13C10, nicotinamide-d4, 1-methylnicotinamide-d3, adenosine-13C5 and GTP-13C10) in a concentration range of 0.0002 to 20 nmol/ml. Muscle tissues were added with water at 2.5 μl/mg raw material and then homogenized on an MM 400 mixer mill for 1 min twice. Methanol

at 7.5 μl/mg raw material was then added and the samples were homogenized for 1 min three times. The samples were then placed at - 20 °C for 2 h before centrifugation. 20 μl of the supernatant was mixed with 180 μl of the internal standard solution. The samples were then placed at 5 °C for 1 h and then centrifuged for 5 min at 21,000 xg. The clear supernatants were used for LC-MS analyses. For metabolomic analyses in PBMCs, several aliquots of one sample were thawed on ice, centrifuged (10 min, 350 xg, 4 °C), resuspended in ice-cold PBS and counted on a countess II cell counter. The equivalent volume of 10 Mio live cells was transferred into a new tube, centrifuged (10 min, 350 xg, 4 °C), the supernatant removed, and the pellet immediately frozen on dry ice. Each PBMC sample was made into 75% methanol at a concentration of 50 μl per 1 Mio cells. After cell lysis on a MM 400 mixer mill for 1 min twice, the sample was centrifuged. 20 μl of the clear supernatant was mixed with 180 μl of the internal standard solution and was then used for LC-MS analysis.

For UPLC-MRM/MS, 10 μl aliquots of each standard solution and each sample solutions were injected to run LCMRM/MS either on a Waters Acquity UPLC coupled to a Sciex QTRAP 6500 Plus mass spectrometer with (-) ion detection or ESI or on an Agilent 1290 UHPLC system coupled to an Agilent 6495B QQQ mass spectrometer with (+) ion detection. For UPLC-(-) MRM/MS, a reversed-phase C18 LC column (2.1*100 mm, 1.8 μm) was used for LC separation, with the use of a tributylamine-ammonium acetate buffer (solvent A) and acetonitrile (solvent B) as the mobile phase for gradient elution at 50 °C and 0.25 ml/min. For UPLC-(+) MRM/MS, a reversed-phase C18 column (2.1*150 mm, 1.8 μm) was used for LC separation, with the use of hepatofluorobutyrate buffer (solvent A) and methanol (solvent B) as the mobile phase for gradient elution at 50 °C and 0.3 ml/min. Concentrations of individual metabolites detected in each sample were calculated by constructing linear-regression curves of individual metabolites with the analyte-to-internal standard peak area ratios (As/Ai) of standard solutions in each set of LC-MS runs and then by interpolating the calibration curves with the as/Ai values measured from injections of sample solutions in an appropriate concentration range for each compound. Sample preparation and metabolomic analyses were conducted at Creative Proteomics, NY, USA.

CSF metabolomics

The extraction of metabolites from CSF samples was carried out as follows: 400 μl of each sample were mixed with 1600 μl of ice-cold UHPLC grade methanol. The samples were vortexed for 10 sec before centrifugation at 16,000 xg for 20 min. 1800 μl of the clear supernatant were transferred to a fresh tube and freeze-dried at -105 °C in a SpeedVac (Thermo Scientific) coupled with a refrigerated vapor trap. The residue was reconstituted in 40 μl of acetonitrile spiked with sulfadimethoxine at a concentration of 50 pg/ml. The samples were then centrifuged at 16,000 xg for 10 min, and the clear supernatants were used for LC-MS analyses. Recovery rate was tested for several relevant nucleotides and determined to be 93%-96%, depending on the nucleotide.

Metabolite analysis was conducted using a Dionex UltiMate 3000 instrument coupled with an electrospray ionization (ESI) QExactive mass spectrometer (Thermo Scientific). The separation of metabolites was achieved on a ZIC-cHILC column (50 x 2.1 mm, 3μm, Merck), which was kept at 40 °C during analysis. The injection volume was 5 μl and the flow rate was kept at 0.3 ml/min. The mobile phase consisted of 10 mM ammonium carbonate pH 8.0, 3 % acetonitrile (solvent A) and 10 mM ammonium carbonate pH 8.0, 90 % acetonitrile (solvent B). The applied gradient was: 85 % B for 0.5 min, decreased to 70 % B during 0.1 min, constant at 70 % B for 1 min, and decreased to 60 % B during 4.3 min. Then, B concentration was decreased to 40 % during 0.1 min, kept at 40 % B for 0.7 min as washout, returned to 85 % B during 0.1 min and was kept for 1.2 min at 85 % B for equilibration prior to the next run. Total run time was 8 min. Electron spray ionization was operated in positive ion polarity mode with a spray voltage of 3.5 kV. Sheath flow gas flow rate was 48 units with an auxiliary gas flow rate of 11 units and a sweep gas flow rate of 2 units. Mass spectra were recorded using targeted single ion monitoring with an isolation window of 10 m/z with automatic gain control set to a target of 5 x 10^5 and a maximum accumulation time of 300 ms. Data analysis was conducted in the Thermo Xcalibur software (Thermo Scientific) using an automated processing method. Absolute concentrations were calculated by external calibration curves using pure standards.

Nf-L, GDF15, FGF21, and Cytokine detection

Neurofilament light chain (Nf-L) measurement in CSF and serum samples was carried out in duplicates using the Simoa NF-light Advantage (SR-X) Kit (Quanterix) according to the manufacturer's recommendations and analyzed on an Simoa SR-X instrument (Quanterix). GDF15 and FGF21 detection was carried out using ELISA kits GDF-15/MIC-1 Human ELISA (RD191135200R) and Fibroblast Growth Factor 21 Human ELISA (RD191108200R) from BioVendor according to manufacturer's recommendations. For CSF analyses of GDF15, CSF was diluted 1:2 in dilution buffer. All samples were analyzed twice in duplicates. Inflammatory Cytokine screening was carried out using the Human Cytokine Magnetic 35-plex panel (Invitrogen), detecting FGF-Basic, IL-1 beta, G-CSF, IL-10, IL-13, IL-6, IL-12, RANTES, Eotaxin, IL-17A, MIP-1 alpha, GM-CSF, MIP-1 beta, MCP-1, IL-15, EGF, IL-5, HGF, VEGF, IL-1 alpha, IFN-gamma, IL-17F, IFN-alpha, IL-9, IL-1RA, TNF-alpha, IL-3, IL-2, IL-7, IP-10, IL-2R, IL-22, MIG, IL-4, IL-8. CSF and serum samples were analyzed according to the manufacturer's recommendations and measured on a BioPlex 200 instrument (BioRad).

QUANTIFICATION AND STATISTICAL ANALYSIS

Sample size

The sample size of 30 participants was chosen based on previous studies of brain metabolic networks using FDG-PET in PD (Lozza et al., 2004; Niethammer et al., 2018; Teune et al., 2013; Wu et al., 2013).

Statistical analyses

The between visit change ([visit 2] - [visit 1]) in MDS-UPDRS (total and subsections I-III) was compared between the NR and placebo groups using independent Student's t test. In addition, the between visit change in MDS-UPDRS (total and subsections) within the NR, MRS-responder, and placebo groups was assessed by paired Student's t test. For the ^{31}P-MRS analyses, the change in measured metabolites between visit 1 and visit 2 was assessed in the placebo- and NR group using paired Student's t test. In addition, the between-visit change in NAD/ATP-α was compared between the NR and placebo group by independent Student's t test. For PET analyses, changes in network scores with treatment were evaluated for each group separately using permutation tests. Relationships between network values, NAD levels and MDS-UPDRS motor ratings or between treatment-related changes in these variables were evaluated using Pearson's product-moment correlations; Spearman rank-order correlation coefficients were computed for non-normal distributions of the variables. These statistical tests were performed using SPSS (SPSS, Chicago, IL); results were considered significant for $p \leq 0.05$ (two-tailed). Metabolite quantification data, Nf-L, GDF15, FGF21 and cytokine data were analyzed by paired sample Wilcoxon test using GraphPad Prism v 6.07. Statistical parameters for conducted analyses can be found in the figures and figure legends. While both sexes were included in our study cohort, there were only five females, one of which was in the placebo group. Therefore, stratification of our analyses by sex was not conducted, due to limited statistical power. The unbalanced sex distribution is a consequence of randomized participant inclusion in the study.

ADDITIONAL RESOURCES

The NAD-PARK trial is registered at Clinicaltrials.gov under the identifier NCT03816020: https://clinicaltrials.gov/ct2/home